

NEURODEGENERATIVE DISORDERS

C9orf72 poly(GR) aggregation induces TDP-43 proteinopathy

Casey N. Cook^{1,2*}, Yanwei Wu^{1*}, Hana M. Odeh^{3*}, Tania F. Gendron^{1,2}, Karen Jansen-West¹, Giulia del Rosso¹, Mei Yue¹, Peizhou Jiang¹, Edward Gomes³, Jimei Tong¹, Lillian M. Daugherty¹, Nicole M. Avendano¹, Monica Castanedes-Casey¹, Wei Shao¹, Björn Oskarsson⁴, Giulio S. Tomassy⁵, Alexander McCampbell⁵, Frank Rigo⁶, Dennis W. Dickson^{1,2}, James Shorter^{3†}, Yong-Jie Zhang^{1,2†}, Leonard Petrucelli^{1,2†}

TAR DNA-binding protein 43 (TDP-43) inclusions are a pathological hallmark of frontotemporal dementia (FTD) and amyotrophic lateral sclerosis (ALS), including cases caused by G₄C₂ repeat expansions in the *C9orf72* gene (c9FTD/ALS). Providing mechanistic insight into the link between *C9orf72* mutations and TDP-43 pathology, we demonstrated that a glycine-arginine repeat protein [poly(GR)] translated from expanded G₄C₂ repeats was sufficient to promote aggregation of endogenous TDP-43. In particular, toxic poly(GR) proteins mediated sequestration of full-length TDP-43 in an RNA-independent manner to induce cytoplasmic TDP-43 inclusion formation. Moreover, in GFP-(GR)₂₀₀ mice, poly(GR) caused the mislocalization of nucleocytoplasmic transport factors and nuclear pore complex proteins. These mislocalization events resulted in the aberrant accumulation of endogenous TDP-43 in the cytoplasm where it co-aggregated with poly(GR). Last, we demonstrated that treating G₄C₂ repeat-expressing mice with repeat-targeting antisense oligonucleotides lowered poly(GR) burden, which was accompanied by reduced TDP-43 pathology and neurodegeneration, including lowering of plasma neurofilament light (NFL) concentration. These results contribute to clarification of the mechanism by which poly(GR) drives TDP-43 proteinopathy, confirm that G₄C₂-targeted therapeutics reduce TDP-43 pathology in vivo, and demonstrate that alterations in plasma NFL provide insight into the therapeutic efficacy of disease-modifying treatments.

INTRODUCTION

Frontotemporal dementia (FTD) is characterized clinically by changes in personality, behavior, and/or language, whereas amyotrophic lateral sclerosis (ALS) is characterized by motor neuron signs. Nevertheless, these two fatal neurodegenerative diseases share pathologic features and genetic causes, and frequently co-occur within the same individuals. FTD and ALS exist on the same disease spectrum and are caused by common pathogenic mechanism(s). A hallmark feature of the vast majority of ALS cases and about half of FTD cases is TAR DNA-binding protein 43 (TDP-43) pathology. TDP-43, a predominantly nuclear DNA/RNA-binding protein with a prion-like domain, plays many roles in RNA metabolism. In patients with FTD/ALS-TDP-43, however, TDP-43 forms cytoplasmic aggregates, which result in its nuclear depletion (1, 2). The underlying factors that initiate these events are unknown, but the discovery of a G₄C₂ repeat expansion in chromosome 9 open reading frame 72 (*C9orf72*) as the most common genetic cause of FTD and ALS (c9FTD/ALS) (3, 4) has provided important insight into potential mechanisms that drive TDP-43 pathology.

In addition to the aggregation of TDP-43, pathological features uniquely derived from the *C9orf72* repeat expansion are observed in

c9FTD/ALS. These include *C9orf72* haploinsufficiency, as well as the accumulation of nuclear RNA foci composed of sense G₄C₂ and antisense G₂C₄ repeat transcripts (3, 5, 6) and dipeptide repeat (DPR) proteins [poly(GA), poly(GP), poly(GR), poly(PR), or poly(PA)] translated from these transcripts through unconventional means (7–11). Several lines of evidence suggest that TDP-43 pathology in c9FTD/ALS results from repeat expansion products rather than loss of *C9orf72*. For instance, knockout of *C9orf72* in mice does not lead to TDP-43 pathology, neurodegeneration, or motor deficits (12). In contrast, mice that express G₄C₂ repeat expansions not only develop RNA foci and express DPR proteins but also exhibit phosphorylated and aggregated endogenous TDP-43 (13–16), indicating that the TDP-43 pathology is likely triggered by repeat RNA and/or DPR proteins produced from the expanded G₄C₂ repeats. Repeat expansion products, especially arginine-rich poly(GR) and poly(PR) proteins, have been implicated in causing nucleocytoplasmic transport defects (17–22) and impairing stress granule (SG) dynamics (13, 23–26), two pathomechanisms linked to TDP-43 mislocalization and aggregation, in c9FTD/ALS. For instance, poly(GR) immunoprecipitates with TDP-43, nucleocytoplasmic transport factors, and SG-associated proteins (26, 27). These findings, along with evidence that essential protein components and key regulators of SG assembly, such as ataxin-2 and T cell intracellular antigen-1 (TIA-1), colocalize with poly(GR) and phosphorylated TDP-43 (pTDP-43) in (G₄C₂)₁₄₉ mice (13), suggest that poly(GR) plays a key role in inducing TDP-43 pathology through the disruption of nucleocytoplasmic transport and SG biology. That poly(GR) colocalizes with TDP-43 inclusions in the motor cortex of patients with c9ALS supports this notion (28). Nonetheless, the mechanistic links between poly(GR) and TDP-43 remain unclear. Here, we used pure protein biochemistry, cell and animal models, as well as human postmortem

¹Department of Neuroscience, Mayo Clinic, Jacksonville, FL 32224, USA. ²Neurobiology of Disease Graduate Program, Mayo Graduate School, Mayo Clinic College of Medicine, Rochester, MN 55902, USA. ³Department of Biochemistry and Biophysics, Perelman School of Medicine, University of Pennsylvania, Philadelphia, PA 19104, USA. ⁴Department of Neurology, Mayo Clinic, Jacksonville, FL 32224, USA. ⁵Neurology Research, Biogen Idec, Cambridge, MA 02142, USA. ⁶Ionis Pharmaceuticals, Carlsbad, CA 92010, USA.

*These authors contributed equally to this work.

†Corresponding author. Email: petrucelli.leonard@mayo.edu (L.P.); zhang.yongjie@mayo.edu (Y.-J.Z.); jshorter@pennmedicine.upenn.edu (J.S.)

brain tissue to investigate the relationship between poly(GR) and TDP-43 proteinopathy.

RESULTS

Poly(GR) accelerates and enhances TDP-43 aggregation

To investigate the relationship between poly(GR) and TDP-43, we first assessed their behavior at the pure protein level. Thus, we incubated purified recombinant maltose-binding protein (MBP)-tagged TDP-43 with or without (GR)₂₀ (a protein with 20 GR repeats) or (GA)₂₀ (a protein with 20 GA repeats). When tagged with MBP, wild-type TDP-43 (TDP-43_{WT}) remained soluble in the absence or presence of (GR)₂₀ or (GA)₂₀ (Fig. 1A). However, after selective removal of the MBP tag by tobacco etch virus (TEV) protease, TDP-43_{WT} formed aggregates in a time-dependent manner (Fig. 1A). Sedimentation analysis at the end point of the turbidity measurements confirmed that the increased absorbance in our aggregation assay is due to the formation of TDP-43_{WT} aggregates (fig. S1A). Upon near completion of MBP cleavage, TDP-43_{WT} in the absence or presence of (GR)₂₀ or (GA)₂₀ fully sedimented into the pellet fraction, whereas free MBP remained soluble (fig. S1A). Of note, co-incubation with (GR)₂₀, but not (GA)₂₀, significantly accelerated and enhanced TDP-43_{WT} aggregation ($P < 0.0001$), although (GR)₂₀ and (GA)₂₀ alone did not aggregate (Fig. 1, A and B). More specifically, (GR)₂₀ elicited the rapid formation of visible, solid-like TDP-43 aggregates at times where no TDP-43 aggregates formed in the presence of buffer or (GA)₂₀ (Fig. 1, A and C). Transmission electron microscopy (TEM) revealed that whereas uncleaved TDP-43_{WT} showed no aggregate formation in the absence or presence of (GR)₂₀ or (GA)₂₀ (fig. S1B), (GR)₂₀ induced the formation of very dense TDP-43_{WT} aggregates upon MBP cleavage (Fig. 1D). In contrast, (GA)₂₀ had no obvious effect on TDP-43, which displayed a typical granulo-filamentous morphology (Fig. 1D). Quantitative analysis revealed that the total area and intensity of TDP-43 aggregates induced by (GR)₂₀ are significantly higher compared to TDP-43 alone ($P < 0.05$) or with (GA)₂₀ ($P = 0.0027$) (Fig. 1E). Collectively, our pure protein studies established that (GR)₂₀ enhances and

accelerates the aggregation of TDP-43 into dense condensates, whereas (GA)₂₀ has no effect.

Poly(GR) recruits cytoplasmic TDP-43 and SG-associated proteins to inclusions

To investigate the effects of poly(GR) aggregates on TDP-43, we first examined the morphology of poly(GR) aggregates using

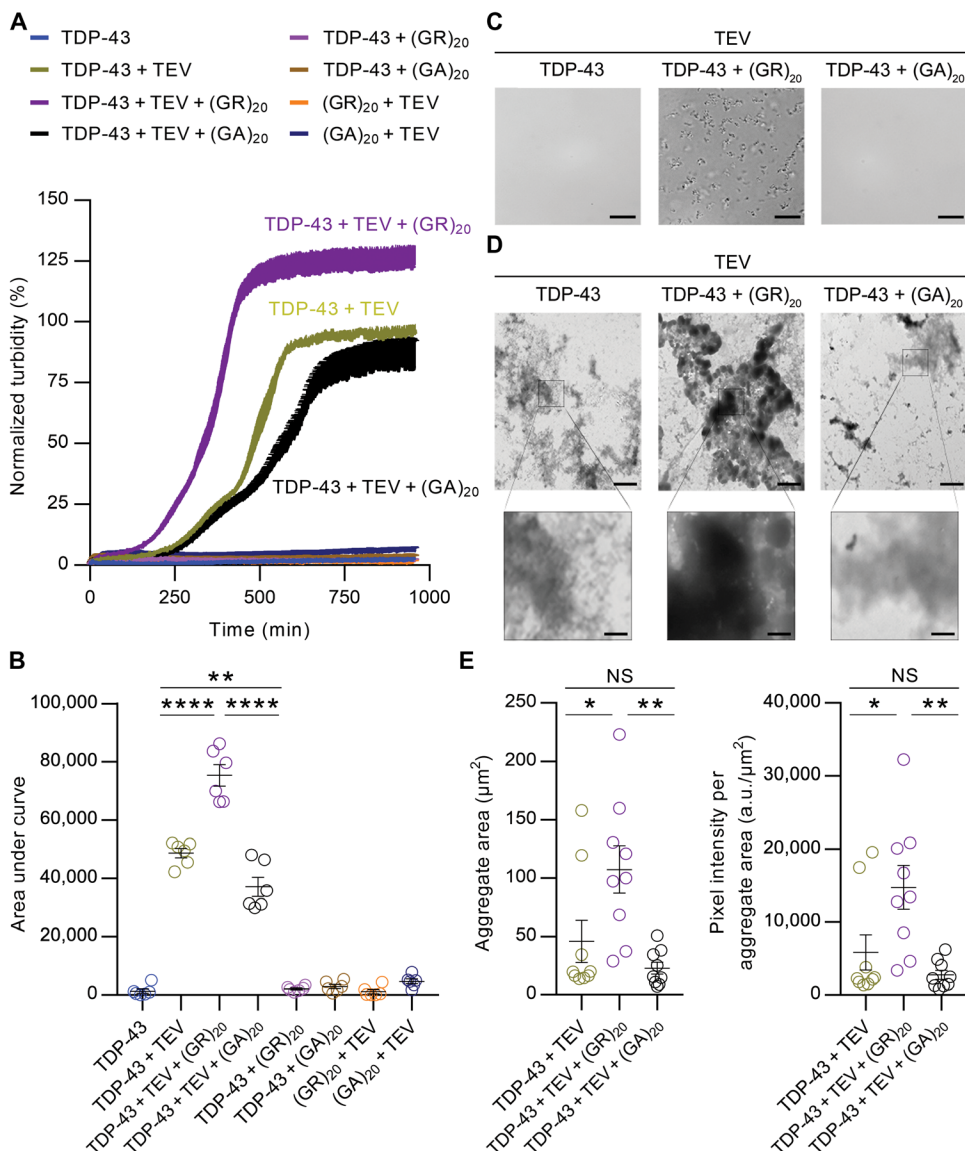


Fig. 1. Poly(GR) directly accelerates and enhances TDP-43 aggregation. (A) TDP-43-MBP (5 μM) was incubated with buffer, 2 μM poly(GR), or 2 μM poly(GA) in the presence or absence of TEV protease (1 μg/ml). Aggregation was assessed by turbidity measured at an absorbance of 395 nm. Values are normalized mean ± SEM ($n = 6$). (B) Quantification of the area under the curve in turbidity for each condition in the in vitro aggregation assay ($n = 6$). (C) TDP-43 aggregation was initiated as described above, with the addition of TEV protease (10 μg/ml) with or without co-incubation with poly(GR) or poly(GA) for 30 min. Aggregation was visualized by differential interference contrast microscopy. Scale bars, 10 μm. (D) Representative electron micrographs of TDP-43 with or without poly(GR) or poly(GA). Samples were processed for EM at the end point of the turbidity assay. Scale bars, 2 μm (top) and 0.4 μm (bottom). (E) EM quantification of TDP-43 aggregate area and intensity per aggregate area with or without poly(GR) or poly(GA) ($n = 9$). Data shown are the mean ± SEM, one-way ANOVA, Tukey's post hoc analysis. In (B), ** $P = 0.0027$ and **** $P < 0.0001$. In (E), * (left to right) $P = 0.0300$ and $P = 0.0263$, ** (left to right) $P = 0.0027$ and $P = 0.0027$, NS (not significant; left to right) $P = 0.5707$ and $P = 0.6080$. a.u., arbitrary units.

immuno-electron microscopy (IEM). We observed gold labeling of poly(GR) antibody on both granular and filamentous materials within cytoplasmic aggregates (Fig. 2A). Following confirmation that poly(GR) forms filaments and granular deposits in transfected cells, human embryonic kidney (HEK) 293T cells expressing green fluorescent protein (GFP) or GFP-tagged (GR)₁₀₀ were cotransfected with various Myc-tagged TDP-43 constructs. Consistent with our previous findings (29), we observed that cytoplasmic GFP-(GR)₁₀₀ inclusions were immunopositive for the SG markers TIA-1, eukaryotic translation initiation factor 3 η (eIF3 η), and ataxin-2 (Fig. 2B and fig. S2A). TDP-43_{WT}, however, was absent from poly(GR)/TIA-1-positive inclusions, instead remaining in the nucleus (Fig. 2, B and C). In contrast, TDP-43 with a mutated nuclear localization signal (TDP-43_{NLSm}) was confined to the cytosol where it co-aggregated with poly(GR) and TIA-1 (Fig. 2, B and C). To confirm that co-aggregation was not merely caused by TDP-43_{NLSm} overexpression, we examined the distribution and expression of TDP-43_{NLSm} in the absence of poly(GR) (fig. S2BD). TDP-43_{NLSm} remained diffusely distributed throughout the cytosol in GFP-transfected cells (Fig. 2C and fig. S2B), despite the fact that TDP-43_{NLSm} expression was higher in GFP-expressing cells than in GFP-(GR)₁₀₀-expressing cells (fig. S2, C and D) [likely because poly(GR) inhibits translation (26, 29)]. Unlike poly(GR), poly(GA) inclusions in GFP-(GA)₁₀₀-expressing cells failed to sequester cytoplasmic TDP-43_{NLSm} (fig. S2E). Together, these data indicate that both the cytoplasmic localization of TDP-43 and its specific recruitment to poly(GR) inclusions promote TDP-43 aggregation.

Given that TDP-43 is an RNA-binding protein, we examined whether cytoplasmic TDP-43 recruitment to GFP-(GR)₁₀₀ inclusions was RNA dependent by mutating five phenylalanine residues within the RNA-binding motifs of TDP-43_{NLSm} to leucine residues (TDP-43_{NLSm-5FL}). Although these mutations disrupt the RNA-binding ability of TDP-43 (30), TDP-43_{NLSm-5FL} nonetheless colocalized to poly(GR) aggregates (Fig. 2, B and C). Next, because the C-terminal prion-like domain of TDP-43 is prone to aggregate (31, 32), we co-expressed TDP-43 C-terminal fragments (CTFs) or TDP-43_{NLSm} lacking the C-terminal domain (TDP-43_{1-273-NLSm}) with GFP-(GR)₁₀₀. Whereas TDP-43_{1-273-NLSm} maintained the ability to be recruited to poly(GR) inclusions (Fig. 2, B and C), TDP-43 CTF formed cytoplasmic aggregates devoid of poly(GR) (fig. S2F). To study the poly(GR)-TDP-43 interaction in more detail, we used a proximity ligation assay (PLA) in which a fluorescent PLA signal is indicative of GFP-(GR)₁₀₀ binding to a given Myc-tagged TDP-43 species. Consistent with a lack of colocalization, no PLA signal was detected in cells expressing GFP-(GR)₁₀₀ and TDP-43_{WT}. In contrast, poly(GR) did interact with cytoplasmic TDP-43_{NLSm}, TDP-43_{NLSm-5FL}, and TDP-43_{1-273-NLSm} as revealed by the positive PLA signal within cytoplasmic poly(GR) inclusions (Fig. 2, D and E). Collectively, our results indicate that poly(GR) interacts with and recruits TDP-43 into inclusions, independent of RNA-binding ability or the aggregation-prone C-terminal prion-like domain of TDP-43.

Poly(GR) aggregates sequester endogenous TDP-43 and SG-resident proteins in vivo

Our cell culture studies indicate that poly(GR) inclusions sequester TDP-43_{NLSm} but not TDP-43_{WT}. This difference raises the possibility that the short experimental period of this cell culture system fails to meet the temporal requirement for poly(GR)-mediated recruitment of TDP-43_{WT}. We therefore examined whether the extended

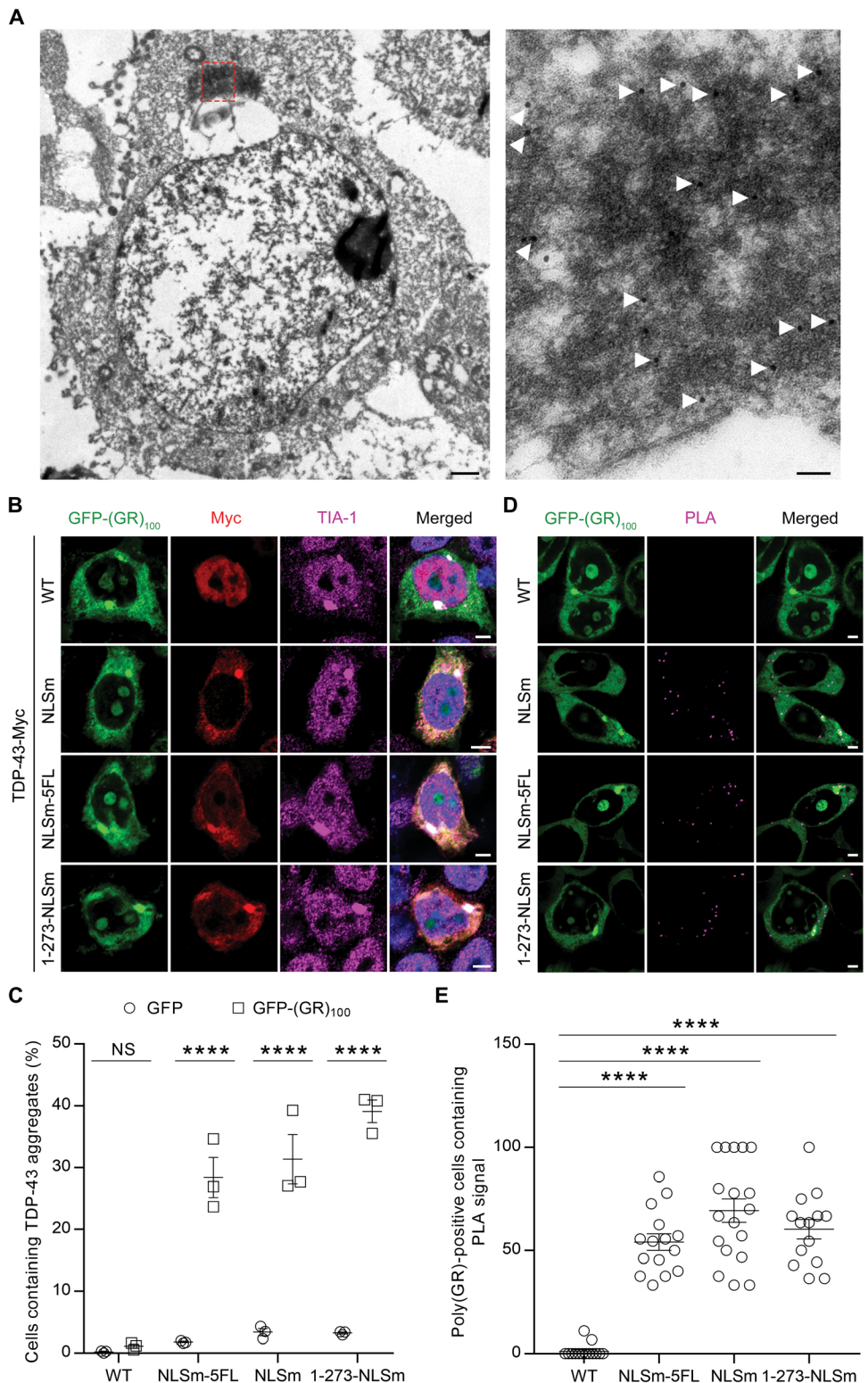
time frame that in vivo studies permit would allow for TDP-43_{WT} to be recruited to poly(GR) aggregates. We recently demonstrated that GFP-(GR)₁₀₀ expression in the brains of mice causes neurodegeneration and translational repression through the binding of poly(GR) to ribosomal subunits and translation initiation factors (29). However, no inclusions of endogenous mouse TDP-43 were observed, which we speculate was due to the lack of GFP-(GR)₁₀₀ aggregation in this model. To overcome this issue, we generated an adeno-associated viral (AAV) construct encoding 200 GR DPRs, which was injected into the lateral ventricles of postnatal day 0 mice. Although poly(GR) predominantly showed a diffuse intracellular distribution in the brains of these mice, poly(GR) aggregates were nonetheless observed in about 7.9 and 3.5% of poly(GR)-positive cells in 2-week-old and 3-month-old mice, respectively (Fig. 3, A and B, and fig. S3A). We detected a significant reduction in the number of diffuse (63.1% decrease, $P < 0.0001$) and aggregated (90.4% decrease, $P = 0.0001$) poly(GR)-positive cells in the cortex from 2 weeks to 3 months of age (Fig. 3B), likely attributed to toxicity of poly(GR) expression and subsequent neuronal loss. Ataxin-2 and TDP-43 aggregates were also observed in brains of GFP-(GR)₂₀₀ mice, but not in GFP mice (Fig. 3, C and D, and fig. S3B). Furthermore, we found that poly(GR) aggregates, but not diffuse poly(GR), colocalized with ataxin-2, eIF3 η , TDP-43, and pTDP-43 (Fig. 3, E to G). Of note, about 95.2 and 78.1% of poly(GR) inclusions in GFP-(GR)₂₀₀ mice were positive for TDP-43 and pTDP-43, respectively (Fig. 3H and fig. S3C). Moreover, consistent with the nuclear depletion of TDP-43 in cells bearing cytoplasmic TDP-43 inclusions in patients with FTD and ALS, significant ($P < 0.0001$) nuclear depletion of TDP-43 was observed in cells containing poly(GR) aggregates compared to non-transduced and diffuse poly(GR)-positive cells (Fig. 3, B, F, and H). Quantitative analysis revealed that about 30.9% of cells containing TDP-43-positive inclusions display TDP-43 nuclear reduction (Fig. 3H), likely reflecting different stages of inclusion formation. We observed poly(GR) inclusions immunopositive for TDP-43 and eIF3 η in c9FTD/ALS patient tissues (Fig. 3I and fig. S3D), and these were accompanied by varying degrees of nuclear TDP-43 depletion. Unlike poly(GR) inclusions in GFP-(GR)₂₀₀ mice, poly(GA) inclusions formed in GFP-(GA)₅₀ mice were negative for TDP-43 and eIF3 η (Fig. 3J), which is consistent with the inability of poly(GA) alone to stimulate TDP-43 aggregation in vitro (Fig. 1) or in cultured cells (fig. S2C). Although poly(GA) is detected within TDP-43 inclusions in c9FTD/ALS postmortem brain tissue (fig. S3E), there is greater colocalization between TDP-43 and poly(GR) (fig. S3F). These results might suggest that poly(GA) colocalizes with TDP-43 in the presence of other G₄C₂-associated pathologies, whereas poly(GR) alone exhibits a unique ability to recruit TDP-43 to inclusions. Together, our data demonstrate that poly(GR) aggregation, in the absence of other G₄C₂-associated pathologies, is sufficient to promote the aggregation of endogenous, wild-type TDP-43 in vivo.

Poly(GR) aggregates sequester nucleocytoplasmic transport factors and nuclear pore complex proteins in vivo

Because the cytoplasmic localization of TDP-43 is required for its sequestration to poly(GR) inclusions, we next determined how endogenous TDP-43 becomes mislocalized in GFP-(GR)₂₀₀ mice. Given that poly(GR) disrupts nucleocytoplasmic transport in yeast, flies, and cultured cells (17, 18, 20), which could disrupt TDP-43 transport to and from the nucleus, we evaluated whether poly(GR) influences nucleocytoplasmic transport factors. We first examined importin α

Fig. 2. Poly(GR) mediates sequestration of cytosolic full-length TDP-43 into the inclusions.

(A) IEM using an anti-poly(GR) antibody labeled with gold particles (18 nm) in HEK293T cells expressing GFP(GR)₁₀₀. The selected region in the low-magnification image (left) is shown at high magnification (right). Scale bars, 1 μm (left) and 0.1 μm (right). (B) Triple-immunofluorescence staining for poly(GR), TDP-43, and TIA-1 in HEK293T cells expressing various GFP-(GR)₁₀₀ and various Myc-tagged TDP-43 species. Scale bars, 5 μm. (C) Quantification of the number of cytoplasmic TDP-43 aggregates in HEK293T cells co-expressing various Myc-tagged TDP-43 constructs with either GFP or GFP-(GR)₁₀₀ (n = 3 independent experiments). (D) Proximity ligation assay (PLA) for GFP-(GR)₁₀₀ and Myc-tagged TDP-43 species in HEK293T cells, with the PLA signal being indicative of their interaction. Scale bars, 5 μm. (E) Quantification of the PLA signal in HEK293T cells expressing GFP-(GR)₁₀₀ and Myc-tagged TDP-43 species (n = 14 to 18 images). Data shown are the mean ± SEM. In (C), ****P < 0.0001 and NS P = 0.9959, two-way ANOVA, Tukey's post hoc analysis. In (E), ****P < 0.0001, one-way ANOVA, Tukey's post hoc analysis. WT, wild type.



and karyopherin α2 (KPNA2), two nuclear import factors that mediate TDP-43 nuclear import (33). Co-immunofluorescence staining demonstrated that the colocalization of poly(GR) and importin α5 or KPNA2 was observed in both diffuse and aggregated poly(GR)-positive cells (Fig. 4A). However, compared to non-transduced cells, aggregated but not diffuse poly(GR) affected the distribution pattern of importin α5 and KPNA2 by recruiting these proteins in poly(GR) inclusions (Fig. 4, A and B). We next assessed various components of the nuclear pore complex (NPC), which consists of about 30 nucleoporins (NUP62, NUP153, NUP214, and NUP358), we observed that NPCs were homogeneously distributed throughout the nuclear envelope in nontransduced and diffuse poly(GR)-positive cells (Fig. 4C). In contrast, in poly(GR) inclusion-bearing cells, NPCs were irregularly distributed around the nuclear envelope and partially colocalized with poly(GR) aggregates, and this was similarly observed for the NPC components NUP98 and pore membrane protein of 121 kDa (POM121) (Fig. 4C and fig. S4). Quantitative analysis revealed that more than 90% of poly(GR) inclusion-bearing cells contained abnormal KPNA2 and NUP98 staining (Fig. 4, B and D). Last, we evaluated whether TDP-43 or eIF3η

distribution was altered in poly(GR)-positive cells with NPC abnormalities. As anticipated, aggregated poly(GR) was associated with aberrant NPC distribution, loss of nuclear TDP-43, and recruitment of cytoplasmic TDP-43 and eIF3η to poly(GR) inclusions

Fig. 3. Poly(GR) aggregation is sufficient to induce mislocalization and aggregation of endogenous TDP-43 in vivo. (A) Representative images of immunohistochemical analysis of poly(GR) in the cortex of 2-week-old GFP mice or GFP-(GR)₂₀₀ mice (diffuse labeling noted by black arrows, aggregates indicated by black arrowheads). Scale bars, 20 μm. (B) Quantification of the number of poly(GR)-positive cells with either diffuse or aggregated poly(GR) in 2-week-old (n = 8) or 3-month-old (n = 7) GFP-(GR)₂₀₀ mice. (C) Representative images of immunohistochemical analysis of ataxin-2 (inclusions indicated by black arrowheads) in the cortex of 2-week-old GFP or GFP-(GR)₂₀₀ mice. (D) Representative images of immunohistochemical analysis of TDP-43 in the cortex of 2-week-old GFP-(GR)₂₀₀ mice. Arrowheads in GFP-(GR)₂₀₀ mice indicate cells with TDP-43-positive inclusions and either normal (left panel) or reduced (right panel) nuclear TDP-43. Scale bars, 20 μm. (E) Double-immunofluorescence staining for poly(GR) and ataxin-2 in the cortex of 2-week-old GFP-(GR)₂₀₀ mice (n = 6). Scale bars, 5 μm. (F) Triple-immunofluorescence staining for eIF3η, TDP-43, and poly(GR) in the cortex of 2-week-old GFP-(GR)₂₀₀ mice (n = 6). Scale bars, 5 μm. (G) Double-immunofluorescence staining for poly(GR) and pTDP-43 in the cortex of 2-week-old GFP-(GR)₂₀₀ mice (n = 6). Scale bars, 5 μm. (H) Quantification of the percentage of cells that are either non-transduced (NT) cells or transduced cells with either diffuse or aggregated poly(GR) that contain TDP-43 inclusions and exhibit depleted nuclear TDP-43 in 2-week-old GFP-(GR)₂₀₀ mice (n = 6). (I) Triple-immunofluorescence staining for poly(GR), eIF3η, and TDP-43 in the hippocampus of patients with c9FTD/ALS [case #1 (top), case #2 (bottom); see table S3 for patient information]. (J) Triple-immunofluorescence staining for poly(GA), eIF3η, and TDP-43 in the cortex of 3-month-old GFP-(GA)₅₀ mice (n = 3). Scale bars, 5 μm. Data shown are the mean ± SEM. In (B), ***P = 0.0001 and ****P < 0.0001, two-tailed unpaired t test. In (H), ****P < 0.0001, one-way ANOVA, Tukey's post hoc analysis.

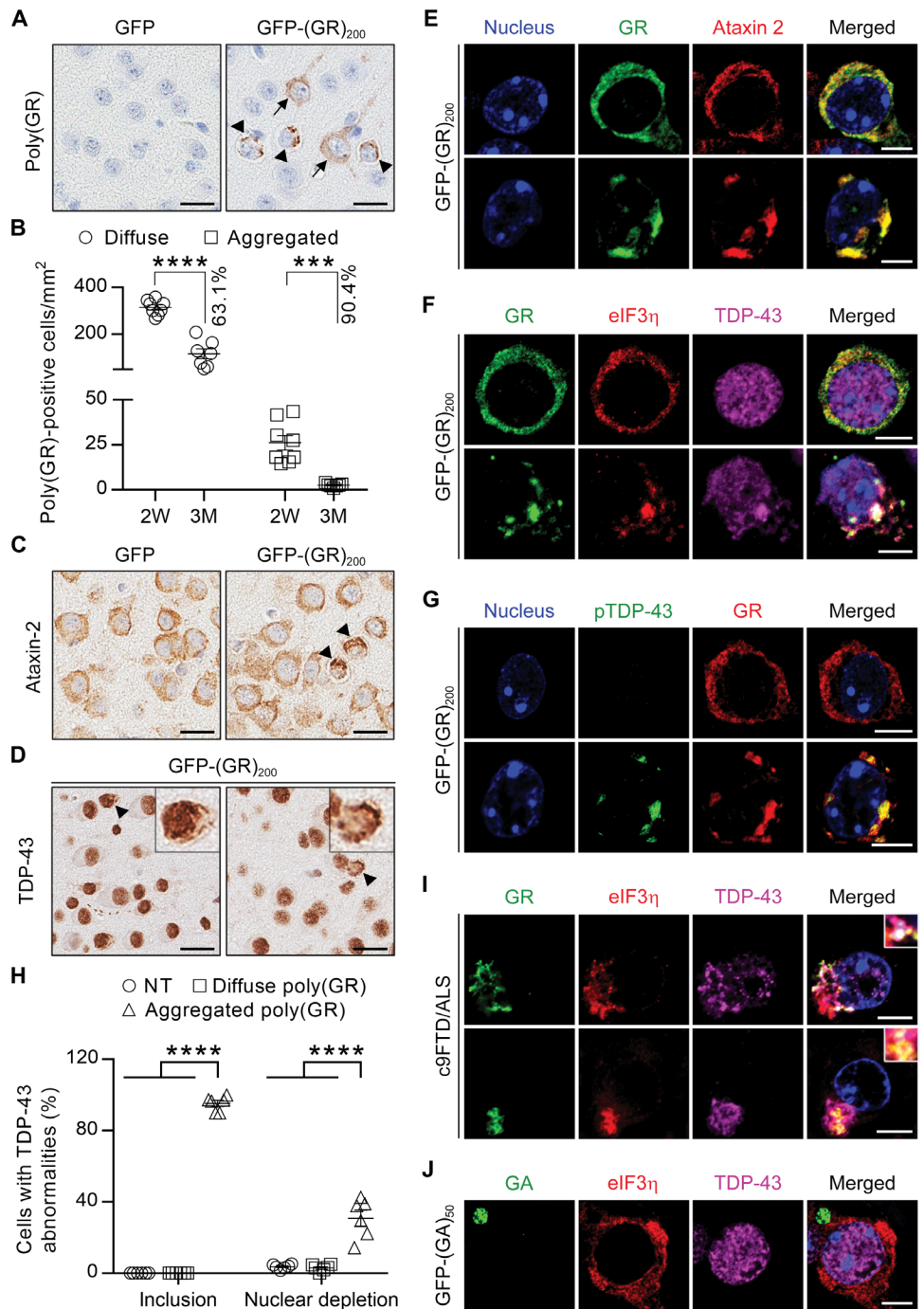


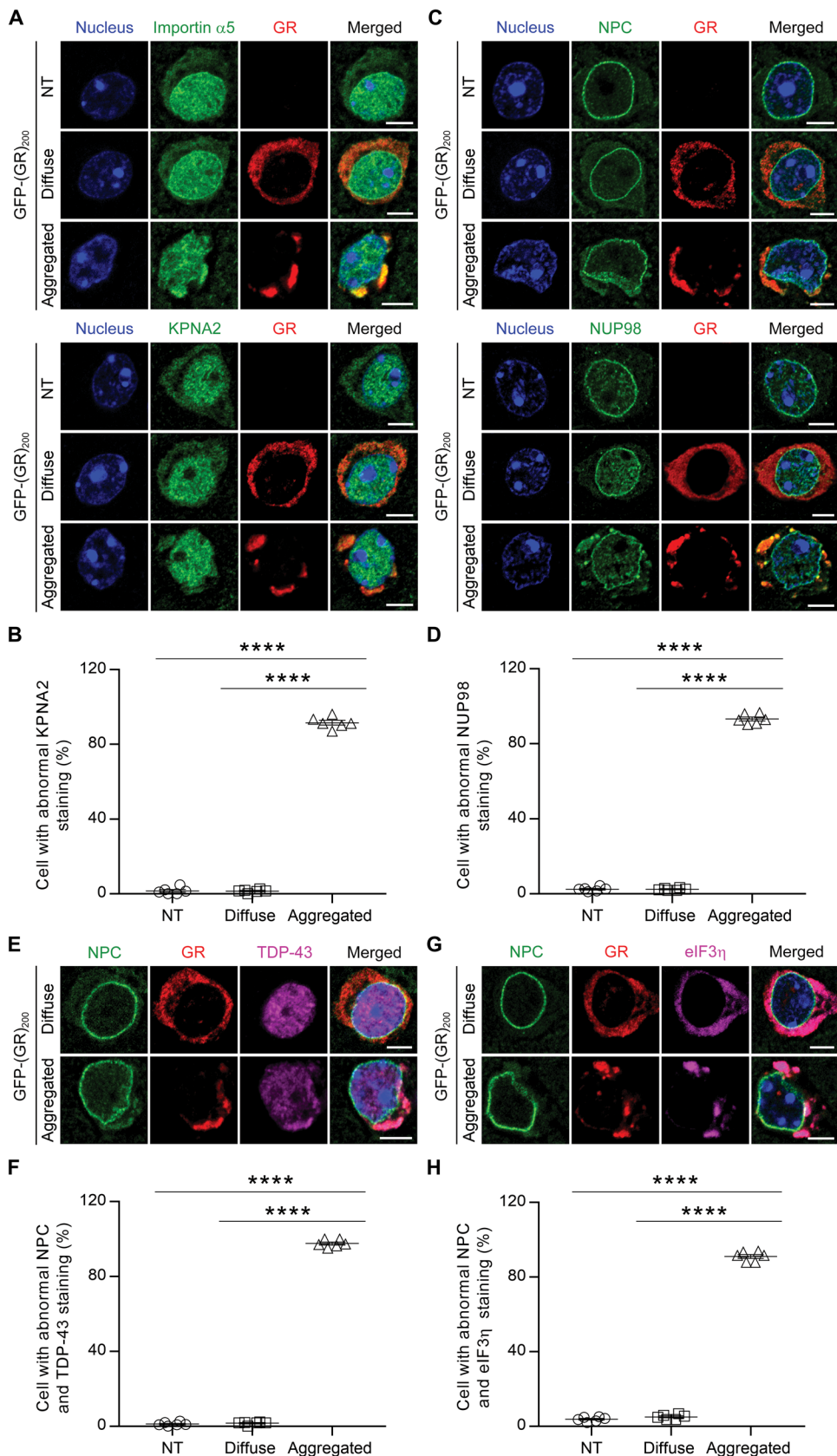
(Fig. 4, E to H). These results provide in vivo evidence that poly(GR) expression alone is sufficient to disturb nucleocytoplasmic transport factors and NPC proteins, contributing to the mislocalization of endogenous, wild-type TDP-43 and ultimately driving TDP-43 proteinopathy.

A G₄C₂-targeted therapeutic mitigates poly(GR) and TDP-43 aggregation and rescues neurodegeneration in vivo

We previously reported that expressing expanded G₄C₂ repeats in the brain of mice leads to the accumulation of repeat-containing transcripts, DPR proteins, and pTDP-43 pathology (13, 14). Data from the present study strongly suggest that poly(GR) is directly responsible for inducing the TDP-43 pathology detected in (G₄C₂)₆₆

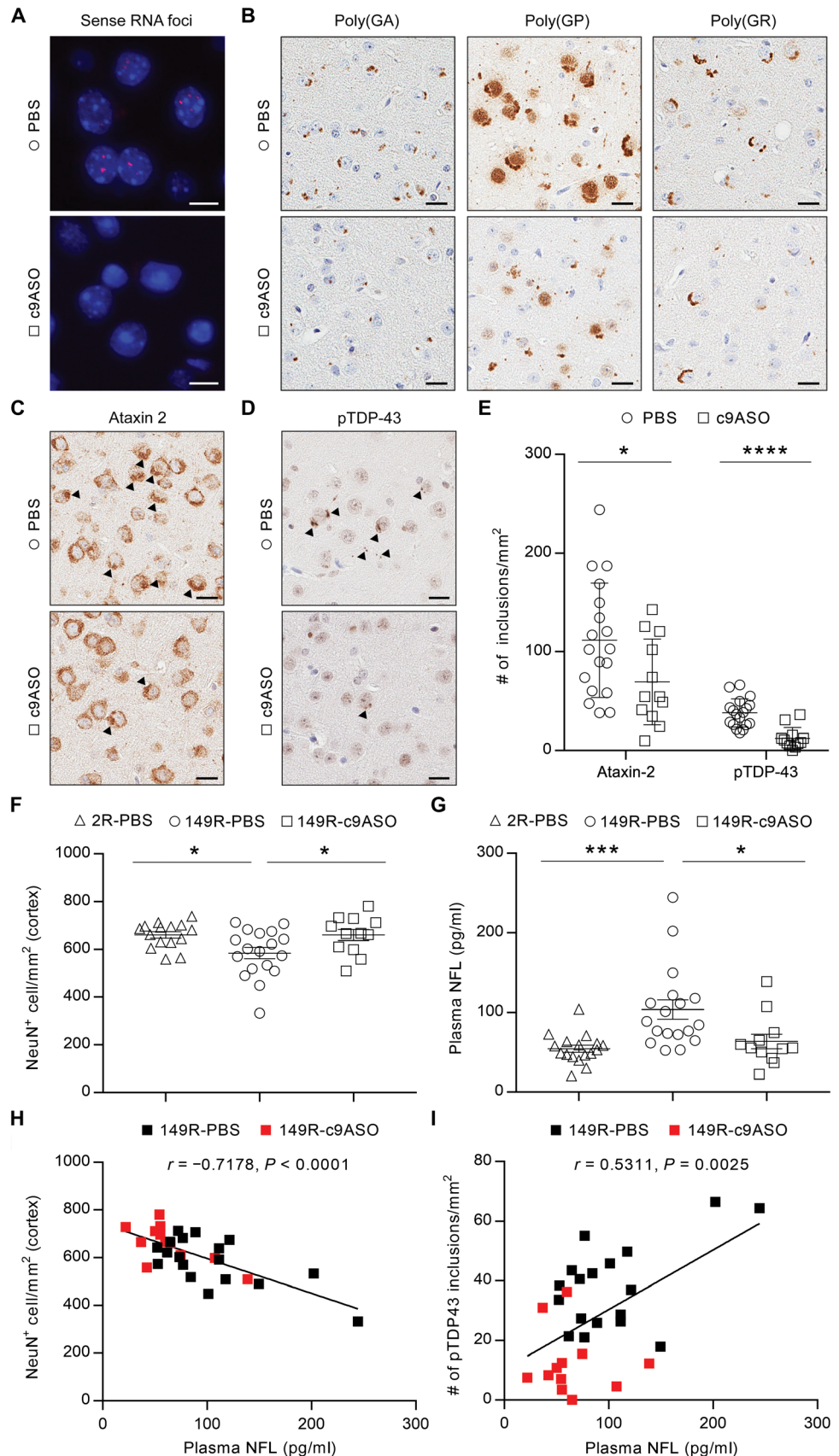
and (G₄C₂)₁₄₉ mice, and this role of poly(GR) is further supported by our previous observation that poly(GR) aggregates in (G₄C₂)₁₄₉ mice are immunopositive for pTDP-43 and TIA-1 (13). Although we have shown that treating (G₄C₂)₆₆ mice with antisense oligonucleotides targeting G₄C₂ repeats (c9ASO) decreases G₄C₂ repeat RNA and DPR protein expression (34), it remains unclear whether c9ASOs, which are currently being tested in clinical trials, will also alleviate pTDP-43 pathology. This issue is critical as it is likely imperative to combat TDP-43 proteinopathy and restore functional TDP-43 to the nucleus to rescue degenerating neurons. To investigate

Fig. 4. Poly(GR) aggregates sequester nucleocytoplasmic transport factors and NPC proteins in vivo. (A) Double-immunofluorescence staining for poly(GR) and importins in nontransduced (NT), diffuse, or aggregated poly(GR) cells, including importin $\alpha 5$ (top three panels) and karyopherin $\alpha 2$ (KNPA2; bottom three panels) in the cortex of 2-week-old GFP-(GR)₂₀₀ mice ($n=6$). Scale bars, 5 μm . (B) Quantification of the percentage of NT cells or of transduced cells with either diffuse or aggregated poly(GR) that contain abnormal KNPA2 in 2-week-old GFP-(GR)₂₀₀ mice ($n=6$). (C) Double-immunofluorescence staining for poly(GR) and several NPC proteins, including NPC (top three panels) and NUP98 (bottom three panels) in the cortex of 2-week-old GFP-(GR)₂₀₀ mice ($n=6$). Scale bars, 5 μm . (D) Quantification of the percentage of NT cells or of transduced cells with either diffuse or aggregated poly(GR) that contain abnormal NUP98 in 2-week-old GFP-(GR)₂₀₀ mice ($n=6$). (E) Triple-immunofluorescence staining for NPC, poly(GR), and TDP-43 in the cortex of GFP-(GR)₂₀₀ mice ($n=6$). Scale bars, 5 μm . (F) Quantification of the percentage of NT cells or of transduced cells with either diffuse or aggregated poly(GR) that contain abnormal NPC and TDP-43 in 2-week-old GFP-(GR)₂₀₀ mice ($n=6$). (G) Triple-immunofluorescence staining for NPC, poly(GR), and eIF3 η in the cortex of 2-week-old GFP-(GR)₂₀₀ mice ($n=6$). Scale bars, 5 μm . (H) Quantification of the percentage of NT cells or of transduced cells with either diffuse or aggregated poly(GR) that contain abnormal NPC and eIF3 η in 2-week-old GFP-(GR)₂₀₀ mice ($n=6$). Data shown are the mean \pm SEM; **** $P < 0.0001$, one-way ANOVA, Tukey's post hoc analysis.



this issue, c9ASOs were injected into the brain of 3-month-old (G₄C₂)₁₄₉ mice, which develop robust RNA foci and DPR protein pathology by this age (13). As anticipated, G₄C₂ repeat-containing RNA expression, assessed by both fluorescence in situ hybridization (FISH) and quantitative reverse transcription polymerase chain reaction (qRT-PCR), was reduced 3 months after treatment (Fig. 5A and fig. S5, A and B). To assess DPR burden, we used both immunohistochemistry of fixed brain tissue and immunoassays of cortical brain lysates, which confirmed that poly(GR) was reduced by c9ASO treatment, along with the other sense DPR proteins poly(GA) and poly(GP) (Fig. 5B and fig. S5C). Moreover, the number of inclusions immunopositive for pTDP-43 or ataxin-2 was also significantly reduced (Fig. 5, C to E; $P < 0.0001$ and $P = 0.0407$ for

Fig. 5. A G_4C_2 -targeting therapeutic reduces poly(GR) and alleviates TDP-43 aggregation and neurodegeneration in vivo. (A) Representative images of RNA FISH for the detection of sense RNA foci in $(G_4C_2)_{149}$ mice treated with PBS or c9ASO. Scale bars, 10 μm . (B) Immunohistochemical labeling of poly(GA), poly(GP), and poly(GR) in PBS- or c9ASO-treated $(G_4C_2)_{149}$ mice. Scale bars, 20 μm . (C and D) Representative images of immunohistochemical analysis of ataxin-2 (C) and pTDP-43 (D) in PBS- or c9ASO-treated $(G_4C_2)_{149}$ mice, with inclusions indicated by black arrowheads. Scale bars, 20 μm . (E) Quantitative analysis of the number of ataxin-2 or pTDP-43 inclusions per square millimeter of cortex in $(G_4C_2)_{149}$ mice treated with PBS ($n = 18$) or c9ASO ($n = 12$). (F) Quantitative analysis of the number of NeuN-positive neurons per square millimeter of cortex in $(G_4C_2)_{149}$ mice treated with PBS ($n = 18$) or c9ASO ($n = 12$) relative to $(G_4C_2)_2$ control mice treated with PBS (2R-PBS, $n = 15$). (G) Plasma neurofilament light (NFL) concentrations in mice measured using the Simoa HD-1 Analyzer (2R-PBS, $n = 17$; 149R-PBS, $n = 18$; 149R-c9ASO, $n = 12$). (H) The number of NeuN-positive neurons per square millimeter of cortex negatively correlated with plasma NFL concentrations in $(G_4C_2)_{149}$ mice (PBS- and c9ASO-treated mice indicated by black and red squares, respectively). (I) The number of pTDP-43 inclusions per square millimeter of cortex positively correlated with plasma NFL concentrations in $(G_4C_2)_{149}$ mice. Data represent the mean \pm SEM. In (E), $*P = 0.0407$ and $****P < 0.0001$, unpaired two-tailed t test. In (F), $*$ (left to right) $P = 0.0293$ and $P = 0.0426$, one-way ANOVA, Tukey's post hoc analysis. In (G), $*P = 0.0166$ and $***P = 0.0009$, one-way ANOVA, Tukey's post hoc analysis.



pTDP-43 and ataxin-2, respectively), validating that reduced poly(GR) and other G_4C_2 -associated pathologies are associated with diminished TDP-43 pathology.

To assess the neuroprotective effect of c9ASO-mediated alleviation of the abovementioned pathologies, we examined both neuronal number and amount of plasma neurofilament light (NFL), a biomarker of neuronal injury (35–37). c9ASO treatment prevented the reduction in NeuN-positive cortical neurons otherwise observed in $(G_4C_2)_{149}$ mice compared to control $(G_4C_2)_2$ mice, which were attenuated in c9ASO-treated $(G_4C_2)_{149}$ mice (Fig. 5F). In addition, we observed increased plasma NFL concentrations in $(G_4C_2)_{149}$ mice compared to control $(G_4C_2)_2$ mice, which were attenuated in c9ASO-treated $(G_4C_2)_{149}$ mice (Fig. 5G). To examine the pathological meaning of alterations in plasma NFL in the $(G_4C_2)_{149}$ model, we evaluated the relationship between plasma NFL and neuronal counts,

as well as TDP-43 pathology. Of note, plasma NFL negatively correlated with the number of NeuN-positive neurons (Fig. 5H) and positively correlated with pTDP-43 pathology (Fig. 5I) in $(G_4C_2)_{149}$ mice, suggesting that plasma NFL concentrations are reflective of neuronal viability and TDP-43 burden in the brain. Together, these findings demonstrate that c9ASO treatment mitigates TDP-43 proteinopathy, which is associated with a reduction in neuronal loss and stabilization of plasma NFL concentrations in vivo.

DISCUSSION

In this study, we uncovered a key role for G_4C_2 repeat-derived poly(GR) in promoting TDP-43 proteinopathy in vitro and in vivo. Specifically, we established that poly(GR) directly accelerates and enhances TDP-43 aggregation. Moreover, poly(GR) sequesters cytoplasmic full-length TDP-43 through an RNA-independent mechanism. In doing so, poly(GR) induces the formation of dense TDP-43 aggregates in vitro. The formation of poly(GR) inclusions immunopositive for TDP-43 and SG-resident proteins in GFP-(GR)₂₀₀ mice demonstrates that poly(GR) aggregation, in the absence of other G_4C_2 -associated pathologies, is sufficient to induce endogenous TDP-43 aggregation. Combined with corroborating findings of inclusions containing both poly(GR) and TDP-43 in patients with c9FTD/ALS, these results provide in vivo validation in both mouse and human postmortem brain tissues that poly(GR) accumulation directly induces TDP-43 proteinopathy.

A key feature of TDP-43 pathology in humans is that TDP-43 inclusions are accompanied by the loss of nuclear TDP-43. Thus, our observation that a subset of neurons with cytoplasmic poly(GR)/TDP-43-positive inclusions exhibited reduced nuclear TDP-43 in GFP-(GR)₂₀₀ mice increases pathological meaning. Given that importins and NPC proteins interact with poly(GR) (20, 26, 27), we asked whether the aberrant cytoplasmic distribution of endogenous TDP-43 in poly(GR)-positive cells might be caused by poly(GR)-induced nucleocytoplasmic transport defects. In support of this idea, we present evidence that several importins and nucleoporins are abnormally distributed in poly(GR)-positive cells and partially colocalize with poly(GR) inclusions in GFP-(GR)₂₀₀ mice. These features were accompanied by both the loss of nuclear TDP-43 and its recruitment to cytoplasmic poly(GR) inclusions. These results support a temporal mechanism in which poly(GR) impairs nucleocytoplasmic transport by sequestering key nucleocytoplasmic transport factors and nucleoporins, which subsequently drives cytoplasmic accumulation and ultimately co-aggregation of TDP-43 with poly(GR) through protein-protein interactions.

Given our observations that poly(GR) alone is sufficient to induce endogenous TDP-43 mislocalization and aggregation, it is noteworthy that both TDP-43 and poly(GR) burden correlate with neurodegeneration in patients (28, 38, 39). Consistent with this notion, we observed an age-dependent loss of poly(GR)-positive cells in GFP-(GR)₂₀₀ mice, suggesting that expression of poly(GR) is toxic to neurons. Moreover, the more marked reduction in aggregated poly(GR) compared to diffuse poly(GR) is likely due to the combination of poly(GR) and TDP-43 abnormalities in cells with poly(GR) inclusions. Therefore, therapeutics targeting poly(GR), TDP-43, or both may be needed to modulate neurotoxicity in c9FTD/ALS. Although the current study demonstrates that c9ASOs reduce TDP-43 pathology in an AAV model of c9FTD/ALS, future studies will be needed to explore the benefit of therapeutic strategies specifically

targeting poly(GR) rather than all G_4C_2 repeat-associated pathologies. Although our results indicate that poly(GA) alone does not cause TDP-43 aggregation at either the pure protein level, in cultured cells, or in the mouse brain, it remains possible that additional products generated from the *C9orf72* repeat expansion (RNA foci and other DPR proteins), either on their own or in combination, contribute to disease pathogenesis. TDP-43 has been shown to colocalize with poly(GA) and poly(GP) inclusions in patients with c9ALS, albeit less frequently than with poly(GR) (28). These findings are consistent with our observations in patients with c9FTD/ALS, suggesting that poly(GR) plays a more direct role in driving TDP-43 inclusion formation. In contrast to poly(GR), poly(GA)-induced TDP-43 pathology may require the presence of other *C9orf72*-associated pathology. It also bears mentioning that because poly(PR) shares similar biophysical properties and functions as poly(GR) (26), it too may also cause TDP-43 aggregation. However, poly(PR) inclusions are rare in patients with c9FTD/ALS (10, 40) and thus unlikely to be a major driver of TDP-43 pathology.

Although our findings reveal a new mechanism to explain TDP-43 pathology in poly(GR)-positive cells, it is important to note that there are other mechanisms underpinning TDP-43 proteinopathy. For example, our results indicate that the aggregation of pathological TDP-43 CTFs is independent of poly(GR) in cultured cells. Moreover, despite the abundance of TDP-43 pathology in the spinal cord of patients with c9ALS, poly(GR) aggregates in this region are rare (41). In addition, two recent studies provide insight into the underlying causes of TDP-43 pathology in sporadic ALS and FTD and/or poly(GR)-negative cells by demonstrating that cytoplasmic TDP-43 aggregation is mediated by aberrant phase transitions and occurs independently of SGs (42, 43). These data suggest that the observed recruitment of SG proteins to poly(GR) aggregates in GFP-(GR)₂₀₀ mice occurs through their direct interaction with poly(GR) rather than by binding TDP-43. This mechanism is also consistent with the identification of the SG proteins RasGAP SH3 domain binding protein 1 (G3BP1) and ataxin-2 as poly(GR)-interacting proteins (26, 27), and with our finding that endogenous TIA-1 is recruited to poly(GR) inclusions in cultured cells expressing nuclear TDP-43_{WT}. Confined to the nucleus, TDP-43_{WT} remains absent from these poly(GR) aggregates. Last, the fact that blocking the RNA-binding ability of TDP-43 disrupts its interaction with ataxin-2 (44) and its localization to SGs (43), but does not prevent its sequestration to poly(GR)-induced aggregates immunopositive for SG proteins, provides compelling evidence that the recruitment of TDP-43 to poly(GR) inclusions is mediated by a direct interaction, rather than its co-aggregation, with cytoplasmic SGs.

Considering that c9ASOs targeting G_4C_2 repeat transcripts are currently being tested in clinical trials, our data showing that c9ASO treatment in $(G_4C_2)_{149}$ mice mitigates poly(GR) burden, TDP-43 pathology, the aberrant SG response, and neurodegeneration are especially relevant. Moreover, we demonstrate that plasma NFL, which is abnormally elevated in $(G_4C_2)_{149}$ mice and reduced with c9ASO treatment, also correlates with neuronal loss and TDP-43 pathology in $(G_4C_2)_{149}$ mice. These results indicate that alterations in plasma NFL concentrations are both reflective of the severity of endogenous TDP-43 pathology in the $(G_4C_2)_{149}$ model and responsive to treatment.

Along with the insights provided by our findings, it is important to acknowledge the limitations of the current study. Although we and others have observed substantial colocalization between TDP-43

and poly(GR) in patients with c9FTD/ALS using TDP-43 antibodies targeting the N-terminal region and phosphorylated serine-409/410 sites (28), additional studies using an array of antibodies targeting different epitopes of the TDP-43 protein in multiple brain regions from a large cohort of c9FTD/ALS patients are warranted. Next, we demonstrated the promising effects of c9ASO treatment in $(G_4C_2)_{149}$ mice. However, as all G_4C_2 repeat-associated pathologies are decreased by c9ASO treatment, additional studies are needed to determine whether the protective effect is mediated by reductions in poly(GR), poly(GA), or G_4C_2 repeat-containing RNA transcripts. In addition, considering that c9ASOs were administered relatively early in the disease course, before substantial pTDP-43 deposition in the $(G_4C_2)_{149}$ mouse model (13), it is unclear whether similar treatment efficacy would be observed if c9ASOs were delivered at a later time point.

In conclusion, we established that poly(GR) potently promotes TDP-43 aggregation through protein-protein interactions (independent of RNA binding and its C-terminal region), sequesters SG-resident proteins and nucleocytoplasmic transport factors, and thus drives TDP-43 proteinopathy in vivo. These pathological features, as well as neuronal loss, can be alleviated by c9ASO treatment. Together, the results of this study establish poly(GR) as a mechanistic link between the *C9orf72* repeat expansion and TDP-43 proteinopathy, and show that decreasing poly(GR) with G_4C_2 -targeted therapeutics is associated with reduced TDP-43 pathology and neurodegeneration in vivo. Moreover, our discovery that plasma NFL in $(G_4C_2)_{149}$ mice correlates with neuronal loss, combined with our previous findings that NFL concentrations in patients with c9FTD correlate with disease severity and brain atrophy (35), indicates that plasma NFL might be used to predict the degree of neurodegeneration. It may also be used to assess efficacy of disease-modifying therapeutics in preclinical models to ultimately guide and facilitate the successful translation of future therapies to humans.

MATERIALS AND METHODS

Study design

The goals of this study were to (i) investigate the role of poly(GR) in driving the cytosolic mislocalization and aggregation of TDP-43 and (ii) determine whether antisense oligonucleotides targeting the G_4C_2 repeat would affect TDP-43 pathology and neurodegeneration in a c9FTD/ALS mouse model. To thoroughly evaluate the mechanistic relationship between poly(GR) and TDP-43, we included in vitro experiments to demonstrate a direct interaction at the pure protein level, cell culture experiments to interrogate cytosolic co-aggregation and the recruitment of SG-associated proteins, and in vivo experiments to assess the ability of poly(GR) to drive accumulation of endogenous mouse TDP-43. To determine whether a therapeutic strategy targeting the G_4C_2 repeat would alleviate TDP-43 proteinopathy and neurodegeneration, we used an AAV-based model that expresses either 2 or 149 G_4C_2 repeats, which we previously demonstrated recapitulates key pathologic features of c9FTD/ALS. At 3 months of age, $(G_4C_2)_{149}$ mice were randomly assigned to either the phosphate-buffered saline (PBS) or c9ASO group, with littermates being assigned to separate groups, and also controlling for gender between groups. Poly(GR) aggregates, TDP-43 inclusions, and *C9orf72*-associated pathologies, as well as nucleocytoplasmic transport factors and NPC protein abnormalities were examined by biochemistry, electron microscopy, immunochemistry, immuno-

fluorescence, FISH, PLA, and immunoassays. Mouse and human samples were randomly selected for analyses. Image analysis was performed in a blinded or unblinded fashion, as detailed in individual experiments. Quantification was performed in a blinded manner. Data from cell culture studies are based on three independent experiments. Group sizes for in vivo studies vary, but are noted in the figure legend. Sample sizes were adequately powered to observe the effects based on previous reports (13, 14, 45–47).

Statistics

All statistical analyses were performed in GraphPad Prism. Data are presented as mean \pm SEM. Data were analyzed by one-way or two-way analysis of variance (ANOVA) followed by Tukey's post hoc analysis, except analyses with two groups were analyzed with two-tailed unpaired *t* test (Figs. 3B and 5E and fig. S3F), and association analyses were performed by determining the Pearson's correlation coefficient (Fig. 5, H and I). Specific tests are also noted in each figure legend. $P < 0.05$ is considered statistically significant.

SUPPLEMENTARY MATERIALS

stm.sciencemag.org/cgi/content/full/12/559/eabb3774/DC1

Materials and Methods

Fig. S1. Poly(GR) accelerates and enhances TDP-43 aggregation.

Fig. S2. Poly(GR) mediates sequestration of cytosolic full-length TDP-43 into the inclusions.

Fig. S3. TDP-43 and DPR burden in mouse and human.

Fig. S4. Poly(GR) aggregates sequester nuclear pore POM121 protein in vivo.

Fig. S5. c9ASO reduces G_4C_2 repeat-containing RNA and sense DPR protein burden.

Table S1. cDNA sequence of the GFP-(GR)₂₀₀ and mCherry-(GR)₁₀₀ plasmids.

Table S2. Primary antibodies for Western blot, immunohistochemistry, and immunofluorescence staining.

Table S3. Characteristics of patients with c9FTD/ALS.

Table S4. Primers for qPCR.

Data file S1. Raw data for all the quantitative figures where $n < 20$.

References (48, 49)

[View/request a protocol for this paper from Bio-protocol.](#)

REFERENCES AND NOTES

1. M. Neumann, D. M. Sampathu, L. K. Kwong, A. C. Truax, M. C. Micsenyi, T. T. Chou, J. Bruce, T. Schuck, M. Grossman, C. M. Clark, L. F. McCluskey, B. L. Miller, E. Masliah, I. R. Mackenzie, H. Feldman, W. Feiden, H. A. Kretzschmar, J. Q. Trojanowski, V. M.-Y. Lee, Ubiquitinated TDP-43 in frontotemporal lobar degeneration and amyotrophic lateral sclerosis. *Science* **314**, 130–133 (2006).
2. T. Arai, M. Hasegawa, H. Akiyama, K. Ikeda, T. Nonaka, H. Mori, D. Mann, K. Tsuchiya, M. Yoshida, Y. Hashizume, T. Oda, TDP-43 is a component of ubiquitin-positive tau-negative inclusions in frontotemporal lobar degeneration and amyotrophic lateral sclerosis. *Biochem. Biophys. Res. Commun.* **351**, 602–611 (2006).
3. M. DeJesus-Hernandez, I. R. Mackenzie, B. F. Boeve, A. L. Boxer, M. Baker, N. J. Rutherford, A. M. Nicholson, N. A. Finch, H. Flynn, J. Adamson, N. Kouri, A. Wojtas, P. Sengdy, G.-Y. R. Hsiung, A. Karydas, W. W. Seeley, K. A. Josephs, G. Coppola, D. H. Geschwind, Z. K. Wszolek, H. Feldman, D. S. Knopman, R. C. Petersen, B. L. Miller, D. W. Dickson, K. B. Boylan, N. R. Graff-Radford, R. Rademakers, Expanded GGGGCC hexanucleotide repeat in noncoding region of *C9ORF72* causes chromosome 9p-linked FTD and ALS. *Neuron* **72**, 245–256 (2011).
4. A. E. Renton, E. Majounie, A. Waite, J. Simón-Sánchez, S. Rollinson, J. R. Gibbs, J. C. Schymick, H. Laaksovirta, J. C. van Swieten, L. Myllykangas, H. Kalimo, A. Paetau, Y. Abramzon, A. M. Remes, A. Kaganovich, S. W. Scholz, J. Duckworth, J. Ding, D. W. Harmer, D. G. Hernandez, J. O. Johnson, K. Mok, M. Ryten, D. Trabzuni, R. J. Guerreiro, R. W. Orrell, J. Neal, A. Murray, J. Pearson, I. E. Jansen, D. Sondervan, H. Seelaar, D. Blake, K. Young, N. Halliwell, J. B. Callister, G. Toulson, A. Richardson, A. Gerhard, J. Snowden, D. Mann, D. Neary, M. A. Nalls, T. Peuralinna, L. Jansson, V.-M. Isoviita, A.-L. Kaivorinne, M. Hölttä-Vuori, E. Ikonen, R. Sulkava, M. Benatar, J. Wu, A. Chiò, G. Restagno, G. Borghero, M. Sabatelli; The ITALSGEN Consortium, D. Heckerman, E. Rogava, L. Zinman, J. D. Rothstein, M. Sendtner, C. Drepper, E. E. Eichler, C. Alkan, Z. Abdullaev, S. D. Pack, A. Dutra, E. Pak, J. Hardy, A. Singleton, N. M. Williams, P. Heutink, S. Pickering-Brown, H. R. Morris, P. J. Tienari, B. J. Traynor, A hexanucleotide repeat expansion in *C9ORF72* is the cause of chromosome 9p21-linked ALS-FTD. *Neuron* **72**, 257–268 (2011).

5. C. Lagier-Tourenne, M. Baughn, F. Rigo, S. Sun, P. Liu, H.-R. Li, J. Jiang, A. T. Watt, S. Chun, M. Katz, J. Qiu, Y. Sun, S.-C. Ling, Q. Zhu, M. Polymeridou, K. Drenner, J. W. Artates, M. McAlonis-Downes, S. Markmiller, K. R. Hutt, D. P. Pizzo, J. Cady, M. B. Harms, R. H. Baloh, S. R. Vandenberg, G. W. Yeo, X.-D. Fu, C. F. Bennett, D. W. Cleveland, J. Ravits, Targeted degradation of sense and antisense *C9orf72* RNA foci as therapy for ALS and frontotemporal degeneration. *Proc. Natl. Acad. Sci. U.S.A.* **110**, E4530–E4539 (2013).
6. S. Mizielińska, T. Lashley, F. E. Norona, E. L. Clayton, C. E. Ridler, P. Fratta, A. M. Isaacs, *C9orf72* frontotemporal lobar degeneration is characterised by frequent neuronal sense and antisense RNA foci. *Acta Neuropathol.* **126**, 845–857 (2013).
7. P. E. A. Ash, K. F. Bieniek, T. F. Gendron, T. Caulfield, W.-L. Lin, M. DeJesus-Hernandez, M. M. van Blitterswijk, K. Jansen-West, J. W. Paul III, R. Rademakers, K. B. Boylan, D. W. Dickson, L. Petrucelli, Unconventional translation of *C9orf72* GGGGCC expansion generates insoluble polypeptides specific to c9FTD/ALS. *Neuron* **77**, 639–646 (2013).
8. K. Mori, T. Arzberger, F. A. Grässer, I. Gijssels, S. May, K. Rentsch, S.-M. Weng, M. H. Schludi, J. van der Zee, M. Cruts, C. Van Broeckhoven, E. Kremmer, H. A. Kretzschmar, C. Haass, D. Edbauer, Bidirectional transcripts of the expanded *C9orf72* hexanucleotide repeat are translated into aggregating dipeptide repeat proteins. *Acta Neuropathol.* **126**, 881–893 (2013).
9. K. Mori, S.-M. Weng, T. Arzberger, S. May, K. Rentsch, E. Kremmer, B. Schmid, H. A. Kretzschmar, M. Cruts, C. Van Broeckhoven, C. Haass, D. Edbauer, The *C9orf72* GGGGCC repeat is translated into aggregating dipeptide-repeat proteins in FTD/ALS. *Science* **339**, 1335–1338 (2013).
10. T. F. Gendron, K. F. Bieniek, Y. J. Zhang, K. Jansen-West, P. E. Ash, T. Caulfield, L. Daugherty, J. H. Dunmore, M. Castanedes-Casey, J. Chew, D. M. Cosio, M. van Blitterswijk, W. C. Lee, R. Rademakers, K. B. Boylan, D. W. Dickson, L. Petrucelli, Antisense transcripts of the expanded *C9orf72* hexanucleotide repeat form nuclear RNA foci and undergo repeat-associated non-ATG translation in c9FTD/ALS. *Acta Neuropathol.* **126**, 829–844 (2013).
11. T. Zu, Y. Liu, M. Bañez-Coronel, T. Reid, O. Pletnikova, J. Lewis, T. M. Miller, M. B. Harms, A. E. Falchook, S. H. Subramony, L. W. Ostrow, J. D. Rothstein, J. C. Troncoso, L. P. W. Ranum, RAN proteins and RNA foci from antisense transcripts in *C9orf72* ALS and frontotemporal dementia. *Proc. Natl. Acad. Sci. U.S.A.* **110**, E4968–E4977 (2013).
12. M. Koppers, A. M. Blokhuis, H.-J. Westeneng, M. L. Terpstra, C. A. C. Zundel, R. Vieira de Sá, R. D. Schellevis, A. J. Waite, D. J. Blake, J. H. Veldink, L. H. van den Berg, R. J. Pasterkamp, *C9orf72* ablation in mice does not cause motor neuron degeneration or motor deficits. *Ann. Neurol.* **78**, 426–438 (2015).
13. J. Chew, C. Cook, T. F. Gendron, K. Jansen-West, G. del Rosso, L. M. Daugherty, M. Castanedes-Casey, A. Kurti, J. N. Stankowski, M. D. Disney, J. D. Rothstein, D. W. Dickson, J. D. Fryer, Y.-J. Zhang, L. Petrucelli, Aberrant deposition of stress granule-resident proteins linked to *C9orf72*-associated TDP-43 proteinopathy. *Mol. Neurodegener.* **14**, 9 (2019).
14. J. Chew, T. F. Gendron, M. Prudencio, H. Sasaguri, Y.-J. Zhang, M. Castanedes-Casey, C. W. Lee, K. Jansen-West, A. Kurti, M. E. Murray, K. F. Bieniek, P. O. Bauer, E. C. Whitelaw, L. Rousseau, J. N. Stankowski, C. Stetler, L. M. Daugherty, E. A. Perkinson, P. Desaro, A. Johnston, K. Overstreet, D. Edbauer, R. Rademakers, K. B. Boylan, D. W. Dickson, J. D. Fryer, L. Petrucelli, *C9orf72* repeat expansions in mice cause TDP-43 pathology, neuronal loss, and behavioral deficits. *Science* **348**, 1151–1154 (2015).
15. J. Jiang, Q. Zhu, T. F. Gendron, S. Saber, M. McAlonis-Downes, A. Seelman, J. E. Stauffer, P. Jafar-Nejad, K. Drenner, D. Schulte, S. Chun, S.-C. Ling, B. Myers, J. Engelhardt, M. Katz, M. Baughn, O. Platoshy, M. Marsala, A. Watt, C. J. Heysler, M. C. Ard, L. DeMuyck, L. M. Daugherty, D. A. Swing, L. Tassarollo, C. J. Jung, A. Delpoux, D. T. Utschneider, S. M. Hedrick, P. J. de Jong, D. Edbauer, P. Van Damme, L. Petrucelli, C. E. Shaw, C. F. Bennett, S. Da Cruz, J. Ravits, F. Rigo, D. W. Cleveland, C. Lagier-Tourenne, Gain of toxicity from ALS/FTD-linked repeat expansions in *C9orf72* is alleviated by antisense oligonucleotides targeting GGGGCC-containing RNAs. *Neuron* **90**, 535–550 (2016).
16. Y. Liu, A. Pattamatta, T. Zu, T. Reid, O. Bardhi, D. R. Borchelt, A. T. Yachnis, L. P. W. Ranum, *C9orf72* BAC mouse model with motor deficits and neurodegenerative features of ALS/FTD. *Neuron* **90**, 521–534 (2016).
17. B. D. Freibaum, Y. Lu, R. Lopez-Gonzalez, N. C. Kim, S. Almeida, K.-H. Lee, N. Badders, M. Valentine, B. L. Miller, P. C. Wong, L. Petrucelli, H. J. Kim, F.-B. Gao, J. P. Taylor, GGGGCC repeat expansion in *C9orf72* compromises nucleocytoplasmic transport. *Nature* **525**, 129–133 (2015).
18. A. Jovičić, J. Mertens, S. Boeynaems, E. Bogaert, N. Chai, S. B. Yamada, J. W. Paul III, S. Sun, J. R. Herdy, G. Bieri, N. J. Kramer, F. H. Gage, L. Van Den Bosch, W. Robberecht, A. D. Gitler, Modifiers of *C9orf72* dipeptide repeat toxicity connect nucleocytoplasmic transport defects to FTD/ALS. *Nat. Neurosci.* **18**, 1226–1229 (2015).
19. K. Zhang, C. J. Donnelly, A. R. Haeusler, J. C. Grima, J. B. Machamer, P. Steinwald, E. L. Daley, S. J. Miller, K. M. Cunningham, S. Vidsensky, S. Gupta, M. A. Thomas, I. Hong, S.-L. Chiu, R. L. Haganir, L. W. Ostrow, M. J. Matunis, J. Wang, R. Sattler, T. E. Lloyd, J. D. Rothstein, The *C9orf72* repeat expansion disrupts nucleocytoplasmic transport. *Nature* **525**, 56–61 (2015).
20. K. Zhang, J. G. Daigle, K. M. Cunningham, A. N. Coyne, K. Ruan, J. C. Grima, K. E. Bowen, H. Wadhwa, P. Yang, F. Rigo, J. P. Taylor, A. D. Gitler, J. D. Rothstein, T. E. Lloyd, Stress granule assembly disrupts nucleocytoplasmic transport. *Cell* **173**, 958–971.e17 (2018).
21. Y. J. Zhang, T. F. Gendron, J. C. Grima, H. Sasaguri, K. Jansen-West, Y.-F. Xu, R. B. Kitzman, J. Gass, M. E. Murray, M. Shinohara, W.-L. Lin, A. Garrett, J. N. Stankowski, L. Daugherty, J. Tong, E. A. Perkinson, M. Yue, J. Chew, M. Castanedes-Casey, A. Kurti, Z. S. Wang, A. M. Liesinger, J. D. Baker, J. Jiang, C. Lagier-Tourenne, D. Edbauer, D. W. Cleveland, R. Rademakers, K. B. Boylan, G. Bu, C. D. Link, C. A. Dickey, J. D. Rothstein, D. W. Dickson, J. D. Fryer, L. Petrucelli, *C9orf72* poly(GA) aggregates sequester and impair HR23 and nucleocytoplasmic transport proteins. *Nat. Neurosci.* **19**, 668–677 (2016).
22. Y.-J. Zhang, L. Guo, P. K. Gonzales, T. F. Gendron, Y. Wu, K. Jansen-West, A. D. O'Raw, S. R. Pickles, M. Prudencio, Y. Carlomagno, M. A. Gachechiladze, C. Ludwig, R. Tian, J. Chew, M. DeTure, W.-L. Lin, J. Tong, L. M. Daugherty, M. Yue, Y. Song, J. W. Andersen, M. Castanedes-Casey, A. Kurti, A. Datta, G. Antognetti, A. McCampbell, R. Rademakers, B. Oskarsson, D. W. Dickson, M. Kampmann, M. E. Ward, J. D. Fryer, C. D. Link, J. Shorter, L. Petrucelli, Heterochromatin anomalies and double-stranded RNA accumulation underlie *C9orf72* poly(PR) toxicity. *Science* **363**, eaav2606 (2019).
23. S. Boeynaems, E. Bogaert, D. Kovacs, A. Konijnenberg, E. Timmerman, A. Volkov, M. Guharoy, M. De Decker, T. Jaspers, V. H. Ryan, A. M. Janke, P. Baatsen, T. Vercurryse, R. M. Kolaitis, D. Daelemans, J. P. Taylor, N. Kedersha, P. Anderson, F. Impens, F. Sobott, J. Schymkowitz, F. Rousseau, N. L. Fawzi, W. Robberecht, P. Van Damme, P. Tompa, L. Van Den Bosch, Phase separation of *C9orf72* dipeptide repeats perturbs stress granule dynamics. *Mol. Cell* **65**, 1044–1055.e5 (2017).
24. W. Cheng, S. Wang, A. A. Mestre, C. Fu, A. Makarem, F. Xian, L. R. Hayes, R. Lopez-Gonzalez, K. Drenner, J. Jiang, D. W. Cleveland, S. Sun, *C9orf72* GGGGCC repeat-associated non-AUG translation is upregulated by stress through eIF2 α phosphorylation. *Nat. Commun.* **9**, 51 (2018).
25. K. M. Green, M. R. Glineburg, M. G. Kearse, B. N. Flores, A. E. Linsalata, S. J. Fedak, A. C. Goldstrohm, S. J. Barmada, P. K. Todd, RAN translation at *C9orf72*-associated repeat expansions is selectively enhanced by the integrated stress response. *Nat. Commun.* **8**, 2005 (2017).
26. K.-H. Lee, P. Zhang, H. J. Kim, D. M. Mitrea, M. Sarkar, B. D. Freibaum, J. Cika, M. Coughlin, J. Messing, A. Mollie, B. A. Maxwell, N. C. Kim, J. Temirov, J. Moore, R.-M. Kolaitis, T. I. Shaw, B. Bai, J. Peng, R. W. Kriwacki, J. P. Taylor, *C9orf72* dipeptide repeats impair the assembly, dynamics, and function of membrane-less organelles. *Cell* **167**, 774–788.e17 (2016).
27. L. R. Hayes, L. Duan, K. Bowen, P. Kalab, J. D. Rothstein, *C9orf72* arginine-rich dipeptide repeat proteins disrupt karyopherin-mediated nuclear import. *eLife* **9**, e51685 (2020).
28. S. Saber, J. E. Stauffer, J. Jiang, S. D. Garcia, A. E. Taylor, D. Schulte, T. Ohkubo, C. L. Schloffman, M. Maldonado, M. Baughn, M. J. Rodriguez, D. Pizzo, D. Cleveland, J. Ravits, Sense-encoded poly-GR dipeptide repeat proteins correlate to neurodegeneration and uniquely co-localize with TDP-43 in dendrites of repeat-expanded *C9orf72* amyotrophic lateral sclerosis. *Acta Neuropathol.* **135**, 459–474 (2018).
29. Y.-J. Zhang, T. F. Gendron, M. T. W. Ebbert, A. D. O'Raw, M. Yue, K. Jansen-West, X. Zhang, M. Prudencio, J. Chew, C. N. Cook, L. M. Daugherty, J. Tong, Y. Song, S. R. Pickles, M. Castanedes-Casey, A. Kurti, R. Rademakers, B. Oskarsson, D. W. Dickson, W. Hu, A. D. Gitler, J. D. Fryer, L. Petrucelli, Poly(GR) impairs protein translation and stress granule dynamics in *C9orf72*-associated frontotemporal dementia and amyotrophic lateral sclerosis. *Nat. Med.* **24**, 1136–1142 (2018).
30. E. Buratti, F. E. Baralle, Characterization and functional implications of the RNA binding properties of nuclear factor TDP-43, a novel splicing regulator of *CFTR* exon 9. *J. Biol. Chem.* **276**, 36337–36343 (2001).
31. Y.-J. Zhang, Y.-F. Xu, C. Cook, T. F. Gendron, P. Roettges, C. D. Link, W.-L. Lin, J. Tong, M. Castanedes-Casey, P. Ash, J. Gass, V. Rangachari, E. Buratti, F. Baralle, T. E. Golde, D. W. Dickson, L. Petrucelli, Aberrant cleavage of TDP-43 enhances aggregation and cellular toxicity. *Proc. Natl. Acad. Sci. U.S.A.* **106**, 7607–7612 (2009).
32. B. S. Johnson, D. Snead, J. J. Lee, J. M. McCaffery, J. Shorter, A. D. Gitler, TDP-43 is intrinsically aggregation-prone, and amyotrophic lateral sclerosis-linked mutations accelerate aggregation and increase toxicity. *J. Biol. Chem.* **284**, 20329–20339 (2009).
33. A. L. Nishimura, V. Župunski, C. Troakes, C. Kathe, P. Fratta, M. Howell, J.-M. Gallo, T. Hortobágyi, C. E. Shaw, B. Rogelj, Nuclear import impairment causes cytoplasmic trans-activation response DNA-binding protein accumulation and is associated with frontotemporal lobar degeneration. *Brain* **133**, 1763–1771 (2010).
34. T. F. Gendron, J. Chew, J. N. Stankowski, L. R. Hayes, Y.-J. Zhang, M. Prudencio, Y. Carlomagno, L. M. Daugherty, K. Jansen-West, E. A. Perkinson, A. O'Raw, C. Cook, L. Pregent, V. Belzil, M. van Blitterswijk, L. J. Tabassian, C. W. Lee, M. Yue, J. Tong, Y. Song, M. Castanedes-Casey, L. Rousseau, V. Phillips, D. W. Dickson, R. Rademakers, J. D. Fryer, B. K. Rush, O. Pedraza, A. M. Caputo, P. Desaro, C. Palmucci, A. Robertson, M. G. Heckman, N. N. Diehl, E. Wiggs, M. Tierney, L. Braun, J. Farren, D. Lacomis, S. Ladha, C. N. Fournier, L. F. McCluskey, L. B. Elman, J. B. Toledo, J. D. McBride, C. Tiloca, C. Morelli, B. Poletti, F. Solca, A. Prelle, J. Wu, J. Jockel-Balsarotti, F. Rigo, C. Ambrose, A. Datta, W. Yang, D. Raitcheva, G. Antognetti, A. McCampbell, J. C. Van Swieten, B. L. Miller, A. L. Boxer,

- R. H. Brown, R. Bowser, T. M. Miller, J. Q. Trojanowski, M. Grossman, J. D. Berry, W. T. Hu, A. Ratti, B. J. Traynor, M. D. Disney, M. Benatar, V. Silani, J. D. Glass, M. K. Floeter, J. D. Rothstein, K. B. Boylan, L. Petrucelli, Poly(GP) proteins are a useful pharmacodynamic marker for C9ORF72-associated amyotrophic lateral sclerosis. *Sci. Transl. Med.* **9**, eaai7866 (2017).
35. L. H. H. Meeter, T. F. Gendron, A. C. Sias, L. C. Jiskoot, S. P. Russo, L. Donker Kaat, J. M. Papma, J. L. Panman, E. L. van der Ende, E. G. Dopfer, S. Franzen, C. Graff, A. L. Boxer, H. J. Rosen, R. Sanchez-Valle, D. Galimberti, Y. A. L. Pijnenburg, L. Benussi, R. Ghidoni, B. Borroni, R. Laforce Jr., M. del Campo, C. E. Teunissen, R. van Minkelen, J. C. Rojas, G. Coppola, D. H. Geschwind, R. Rademakers, A. M. Karydas, L. Oijerstedt, E. Scarpini, G. Binetti, A. Padovani, D. M. Cash, K. M. Dick, M. Bocchetta, B. L. Miller, J. D. Rohrer, L. Petrucelli, J. C. van Swieten, S. E. Lee, Poly(GP), neurofilament and grey matter deficits in C9orf72 expansion carriers. *Ann. Clin. Transl. Neurol.* **5**, 583–597 (2018).
36. L. Gaetani, K. Blennow, P. Calabresi, M. Di Filippo, L. Parnetti, H. Zetterberg, Neurofilament light chain as a biomarker in neurological disorders. *J. Neurol. Neurosurg. Psychiatry* **90**, 870–881 (2019).
37. P. Shahim, H. Zetterberg, Y. Tegner, K. Blennow, Serum neurofilament light as a biomarker for mild traumatic brain injury in contact sports. *Neurology* **88**, 1788–1794 (2017).
38. N. Sakae, K. F. Bieniek, Y.-J. Zhang, K. Ross, T. F. Gendron, M. E. Murray, R. Rademakers, L. Petrucelli, D. W. Dickson, Poly-GR dipeptide repeat polymers correlate with neurodegeneration and clinicopathological subtypes in C9ORF72-related brain disease. *Acta Neuropathol. Commun.* **6**, 63 (2018).
39. I. R. Mackenzie, T. Arzberger, E. Kremmer, D. Troost, S. Lorenzl, K. Mori, S.-M. Weng, C. Haass, H. A. Kretschmar, D. Edbauer, M. Neumann, Dipeptide repeat protein pathology in C9ORF72 mutation cases: Clinic-pathological correlations. *Acta Neuropathol.* **126**, 859–879 (2013).
40. I. R. A. Mackenzie, P. Frick, F. A. Grässer, T. F. Gendron, L. Petrucelli, N. R. Cashman, D. Edbauer, E. Kremmer, J. Prudlo, D. Troost, M. Neumann, Quantitative analysis and clinico-pathological correlations of different dipeptide repeat protein pathologies in C9ORF72 mutation carriers. *Acta Neuropathol.* **130**, 845–861 (2015).
41. J. Gomez-Deza, Y.-b. Lee, C. Troakes, M. Nolan, S. Al-Sarraj, J.-M. Gallo, C. E. Shaw, Dipeptide repeat protein inclusions are rare in the spinal cord and almost absent from motor neurons in C9ORF72 mutant amyotrophic lateral sclerosis and are unlikely to cause their degeneration. *Acta Neuropathol. Commun.* **3**, 38 (2015).
42. F. Gasset-Rosa, S. Lu, H. Yu, C. Chen, Z. Melamed, L. Guo, J. Shorter, S. Da Cruz, D. W. Cleveland, Cytoplasmic TDP-43 de-mixing independent of stress granules drives inhibition of nuclear import, loss of nuclear TDP-43, and cell death. *Neuron* **102**, 339–357.e7 (2019).
43. J. R. Mann, A. M. Gleixner, J. C. Mauna, E. Gomes, M. R. DeChellis-Marks, P. G. Needham, K. E. Copley, B. Hurtle, B. Portz, N. J. Pyles, L. Guo, C. B. Calder, Z. P. Wills, U. B. Pandey, J. K. Kofler, J. L. Brodsky, A. Thathiah, J. Shorter, C. J. Donnelly, RNA binding antagonizes neurotoxic phase transitions of TDP-43. *Neuron* **102**, 321–338.e8 (2019).
44. A. C. Elden, H.-J. Kim, M. P. Hart, A. S. Chen-Plotkin, B. S. Johnson, X. Fang, M. Armakola, F. Geser, R. Greene, M. M. Lu, A. Padmanabhan, D. Clay-Falcone, L. McCluskey, L. Elman, D. Jühr, P. J. Gruber, U. Rüb, G. Auburger, J. Q. Trojanowski, V. M.-Y. Lee, V. M. Van Deerlin, N. M. Bonini, A. D. Gitler, Ataxin-2 intermediate-length polyglutamine expansions are associated with increased risk for ALS. *Nature* **466**, 1069–1075 (2010).
45. L. Guo, H. J. Kim, H. Wang, J. Monaghan, F. Freyermuth, J. C. Sung, K. O'Donovan, C. M. Fare, Z. Diaz, N. Singh, Z. C. Zhang, M. Coughlin, E. A. Sweeney, M. E. DeSantis, M. E. Jackrel, C. B. Rodell, J. A. Burdick, O. D. King, A. D. Gitler, C. Lagier-Tourenne, U. B. Pandey, Y. M. Choock, J. P. Taylor, J. Shorter, Nuclear-import receptors reverse aberrant phase transitions of RNA-binding proteins with prion-like domains. *Cell* **173**, 677–692.e20 (2018).
46. A. Wang, A. E. Conicella, H. B. Schmidt, E. W. Martin, S. N. Rhoads, A. N. Reeb, A. Nourse, D. Ramirez Montero, V. H. Ryan, R. Rohatgi, F. Shewmaker, M. T. Naik, T. Mittag, Y. M. Ayala, N. L. Fawzi, A single N-terminal phosphomimic disrupts TDP-43 polymerization, phase separation, and RNA splicing. *EMBO J.* **37**, e97452 (2018).
47. Y.-J. Zhang, T. Caulfield, Y.-F. Xu, T. F. Gendron, J. Hubbard, C. Stetler, H. Sasaguri, E. C. Whitelaw, S. Cai, W. C. Lee, L. Petrucelli, The dual functions of the extreme N-terminus of TDP-43 in regulating its biological activity and inclusion formation. *Hum. Mol. Genet.* **22**, 3112–3122 (2013).
48. M. Prudencio, K. R. Jansen-West, W. C. Lee, T. F. Gendron, Y.-J. Zhang, Y.-F. Xu, J. Gass, C. Stuani, C. Stetler, R. Rademakers, D. W. Dickson, E. Buratti, L. Petrucelli, Misregulation of human sortilin splicing leads to the generation of a nonfunctional progranulin receptor. *Proc. Natl. Acad. Sci. U.S.A.* **109**, 21510–21515 (2012).
49. T. F. Gendron, M. van Blitterswijk, K. F. Bieniek, L. M. Daugherty, J. Jiang, B. K. Rush, O. Pedraza, J. A. Lucas, M. E. Murray, P. Desaro, A. Robertson, K. Overstreet, C. S. Thomas, J. E. Crook, M. Castanedes-Casey, L. Rousseau, K. A. Josephs, J. E. Parisi, D. S. Knopman, R. C. Petersen, B. F. Boeve, N. R. Graff-Radford, R. Rademakers, C. Lagier-Tourenne, D. Edbauer, D. W. Cleveland, D. W. Dickson, L. Petrucelli, K. B. Boylan, Cerebellar c9RAN proteins associate with clinical and neuropathological characteristics of C9ORF72 repeat expansion carriers. *Acta Neuropathol.* **130**, 559–573 (2015).

Acknowledgments: We are grateful to all patients who agreed to donate postmortem tissue. We thank W.-L. Lin for IEM study. We thank S. Boeynaems for providing the (GR)₂₀ and (GA)₂₀ peptides. **Funding:** This work was supported by the NIH (R35NS097273 to L.P.; P01NS084974 to D.W.D., T.F.G., Y.-J.Z., and L.P.; P01NS099114 to T.F.G. and L.P.; R01NS088689 to L.P.; and R21AG065854 and R01GM099836 to J.S.), Mayo Clinic Foundation (to L.P.), Amyotrophic Lateral Sclerosis Association (to T.F.G., L.P., J.S., and Y.-J.Z.), Robert Packard Center for ALS Research at Johns Hopkins (to L.P. and J.S.), Target ALS Foundation (to T.F.G., L.P., J.S., and Y.-J.Z.), Biogen Idec (to L.P.), and AstraZeneca postdoctoral fellowship (to H.M.O.). **Author contributions:** L.P., Y.-J.Z., J.S., C.N.C., Y.W., and H.M.O. contributed to the conception and design. C.N.C., Y.W., G.d.R., M.Y., J.T., N.M.A., M.C.-C., W.S., G.S.T., A.M., and Y.-J.Z. contributed to mouse and cell studies. P.J. contributed to IEM study. H.M.O. and E.G. conducted the in vitro pure protein studies. Y.W., K.J.-W., and Y.-J.Z. made plasmids. K.J.-W. and L.M.D. prepared AAV virus. F.R. provided c9ASO. B.O. and D.W.D. contributed to the collection of human samples. L.P., Y.-J.Z., C.N.C., Y.W., T.F.G., H.M.O., and J.S. analyzed data and wrote the manuscript. **Competing interests:** B.O. has consulted for Biogen, Medicinova, Mitsubishi, Amylyx, and Tsumura. F.R. is a paid employee of Ionis Pharmaceuticals. G.S.T. and A.M. are paid employees of Biogen Idec. L.P. is a consultant for Expansion Therapeutics. Other authors declare no competing interests. **Data and materials availability:** c9ASOs were provided by Ionis Pharmaceuticals (F.R.) and are covered under a material transfer agreement (MTA). All data associated with this study are available in the main text or the Supplementary Materials. All requests for reagents should be made to the corresponding authors upon reasonable request. They will be made available through appropriate administrative channels (MTA).

Submitted 20 February 2020
Accepted 19 June 2020
Published 2 September 2020
10.1126/scitranslmed.abb3774

Citation: C. N. Cook, Y. Wu, H. M. Odeh, T. F. Gendron, K. Jansen-West, G. del Rosso, M. Yue, P. Jiang, E. Gomes, J. Tong, L. M. Daugherty, N. M. Avendano, M. Castanedes-Casey, W. Shao, B. Oskarsson, G. S. Tomassy, A. McCampbell, F. Rigo, D. W. Dickson, J. Shorter, Y.-J. Zhang, L. Petrucelli, C9orf72 poly(GR) aggregation induces TDP-43 proteinopathy. *Sci. Transl. Med.* **12**, eabb3774 (2020).

Supplementary Materials for

***C9orf72* poly(GR) aggregation induces TDP-43 proteinopathy**

Casey N. Cook, Yanwei Wu, Hana M. Odeh, Tania F. Gendron, Karen Jansen-West, Giulia del Rosso, Mei Yue, Peizhou Jiang, Edward Gomes, Jimei Tong, Lillian M. Daugherty, Nicole M. Avendano, Monica Castanedes-Casey, Wei Shao, Björn Oskarsson, Giulio S. Tomassy, Alexander McCampbell, Frank Rigo, Dennis W. Dickson, James Shorter*, Yong-Jie Zhang*, Leonard Petrucelli*

*Corresponding author. Email: petrucelli.leonard@mayo.edu (L.P.); zhang.yongjie@mayo.edu (Y.-J.Z.); jshorter@pennmedicine.upenn.edu (J.S.)

Published 2 September 2020, *Sci. Transl. Med.* **12**, eabb3774 (2020)
DOI: 10.1126/scitranslmed.abb3774

The PDF file includes:

Materials and Methods

Fig. S1. Poly(GR) accelerates and enhances TDP-43 aggregation.

Fig. S2. Poly(GR) mediates sequestration of cytosolic full-length TDP-43 into the inclusions.

Fig. S3. TDP-43 and DPR burden in mouse and human.

Fig. S4. Poly(GR) aggregates sequester nuclear pore POM121 protein in vivo.

Fig. S5. c9ASO reduces G₄C₂ repeat-containing RNA and sense DPR protein burden.

Table S1. cDNA sequence of the GFP-(GR)₂₀₀ and mCherry-(GR)₁₀₀ plasmids.

Table S2. Primary antibodies for Western blot, immunohistochemistry, and immunofluorescence staining.

Table S3. Characteristics of patients with c9FTD/ALS.

Table S4. Primers for qPCR.

Legend for Data file S1

References (48, 49)

Other Supplementary Material for this manuscript includes the following:

(available at stm.sciencemag.org/cgi/content/full/12/559/eabb3774/DC1)

Data file S1 (Microsoft Excel format). Raw data for all the quantitative figures where $n < 20$.

$\mu\text{g/ml}$ TEV protease to samples. After 30 minutes, 10 μl of sample was mounted onto a glass slide and imaged by differential interference contrast (DIC) microscopy.

In vitro sedimentation assay

At the end point of the turbidity assay described above ($t = 16$ hours), samples were sedimented by centrifugation for 10 minutes at $21,130 \times g$. Pellet and supernatant were immediately separated and equal volumes of each fraction were analyzed by SDS-PAGE. Proteins were visualized by Coomassie stain.

Transmission electron microscopy

Transmission electron microscopy (TEM) was performed as previously described (45). Briefly, at the start of the aggregation assay described above ($t = 0$), and at the end point of the turbidity assay ($t = 16$ hours), 10 μl of each sample was adsorbed onto a 300-mesh Formvar/carbon-coated copper grids (Electron Microscopy Sciences) and stained with 2% (w/v) uranyl acetate. Excess uranyl acetate was washed with water and the grids were allowed to air dry. Samples were viewed and imaged using JEOL 1010 transmission electron microscope. Electron micrographs were quantified using ImageJ. Images were inverted to have a black background. Scale was set to 110 pixels/ μm , based on the scale bar of the micrographs. Threshold was used to determine the region of interest (ROI), which was considered as the total area occupied by TDP-43 aggregates. Total area (μm^2), mean gray value (a.u.), and integrated density were measured, limited to thresholded area. The integrated density, which is the product of the area of the ROI of TDP-43 aggregates and mean gray value of pixel intensity, was reported. For each condition, 9 representative micrographs were quantified, collected from 3 independent experiments.

Generation of plasmids

To generate GFP-(GR)₂₀₀ and mCherry-(GR)₁₀₀ plasmids, a gene fragment containing 50 repeats of the dipeptide GR was synthesized by GeneArt and used as a template for PCR to generate fragments containing one or two Type IIS restriction enzyme sites. These fragments were ligated together sequentially to generate 100 or 200 GR repeats. The coding sequence for EGFP was cloned into the modified AAV packaging vector [pAM/CBA-pl-WPRE-BGH (“pAAV”)] containing the CMV-enhanced chicken β -actin promoter, and (GR)₂₀₀ was ligated in frame downstream of EGFP to generate pAAV EGFP-(GR)₂₀₀. The mCherry coding sequence was amplified using PCR and cloned into the AgeI and HindIII sites of pEGFP-C1, creating the vector mCherry-C1. A (GR)₁₀₀ fragment was ligated in frame downstream of the mCherry to generate mCherry-(GR)₁₀₀. The sequence of GFP-(GR)₂₀₀ and mCherry-(GR)₁₀₀ are listed in **Table S1**, respectively. To generate TDP-43-Myc plasmids, complementary DNA (cDNA) from constructs for wild-type TDP-43 or for TDP-43 with mutations in the nuclear localization signal (NLS) and/or the RNA recognition motifs (RRMs) (47, 48) was used as the PCR template to generate TDP-43 fragments. These fragments were cloned into the HindIII and XhoI sites of

pAG3-Myc vector. The sequences of all plasmids were verified by sequence analysis.

Cell culture and treatments

HEK293T cells were grown in Opti-Mem plus 10% FBS and 1% penicillin–streptomycin. Cells grown in 6-well plates or on glass coverslips in 24-well plates were transfected with the indicated plasmids using Lipofectamine 2000 (Thermo Fisher Scientific). Cells were harvested or fixed for Western blot and immunofluorescence staining, respectively, 24 hours post-transfection.

Immunofluorescence staining and quantification in cultured cells

Fixed cells were permeabilized with 0.5% Triton X-100 for 10 minutes, blocked with 5% nonfat dry milk in PBS for 1 hour, then incubated with primary antibody (**Table S2**) overnight at 4°C. After washing, cells were incubated with corresponding Alexa Fluor 488-, 568- or 647-conjugated donkey anti-species antibodies (1:500 or 1:1000, Molecular Probes) for 2 hours. Hoechst 33258 (1 µg/ml, H3569, Thermo Fisher Scientific) was used to stain cellular nuclei. Images were obtained on a Zeiss LSM 880 laser scanning confocal microscope. To quantify the percentage of cells with cytoplasmic TDP-43 inclusions in GFP- or poly(GR)-positive cells, the number of TDP-43-positive cells containing diffuse or aggregated TDP-43 was counted in a blinded fashion from 3 independent experiments (~500–1000 cells were counted for each group in each independent experiment). To quantify the percentage of cells with cytoplasmic TDP-43 inclusions in poly(GA)-positive cells, the number of TDP-43-positive cells containing diffuse or aggregated TDP-43 was counted in a blinded fashion from 3 independent experiments (~110–190 poly(GA) inclusions were counted for each group in each independent experiment).

Preparation of cell lysates

Cell pellets were lysed in co-immunoprecipitation (co-IP) buffer (50 mM Tris–HCl, pH 7.4, 300 mM NaCl, 1% Triton X-100, 5 mM EDTA) plus 2% SDS, and both protease and phosphatase inhibitors, sonicated on ice, and then centrifuged at 16,000 × g for 20 minutes. Supernatants were saved as cell lysates. The protein concentration of lysates was determined by BCA assay (Thermo Fisher Scientific), and samples were then subjected to Western blot analysis.

Western blot analysis

Cell lysates were diluted with 2× SDS-loading buffer at a 1:1 ratio (v/v), and then heated at 95°C for 5 minutes. Afterwards, equal amounts of protein were loaded into 10-well 4–20% Tris-glycine gels (Novex). After transferring proteins to PVDF membranes, membranes were blocked with 5% nonfat dry milk in TBS plus 0.1% Tween 20 (TBST) for 1 hour, and then incubated with primary antibody (**Table S2**) overnight at 4°C. Membranes were washed in TBST and incubated with donkey anti-rabbit or anti-mouse IgG antibodies conjugated to horseradish peroxidase (1:5000; Jackson ImmunoResearch) for 1 hour. Protein expression was

visualized by enhanced chemiluminescence treatment and exposure to film. The intensity of bands was quantified by FUJI FILM MultiGauge Software, and then normalized to the corresponding controls.

Proximity ligation assay (PLA)

HEK293T cells grown in an 8-well chamber slide (ibidi) were transfected with the indicated plasmids using Lipofectamine 2000 (Life Technologies). Twenty-four hours after transfection, cells were fixed for the PLA study using the Duolink In Situ kit (DUO92004, DUO92002, Sigma-Aldrich) per the manufacturer's protocol. In brief, fixed cells were permeabilized with 0.1% Triton X-100 for 10 minutes, blocked using Duolink blocking buffer for 1 hour at room temperature, and then incubated with rabbit polyclonal anti-GR (Rb7810, 1:2000) (10) and mouse monoclonal anti-Myc (MA1-980, 1:1000, Invitrogen) overnight at 4°C. After washing with PBS plus 0.05% Tween 20, cells were incubated with the PLA probes MINUS and PLUS (1:5 dilution) for 1 hour at 37°C. After washing in 1× wash buffer A, cells were incubated with the ligase (1:40 dilution) in ligation buffer for 30 minutes at 37°C. Cells were washed with 1× wash buffer A, and then inoculated with polymerase (1:80 dilution) in amplification buffer for 90 minutes at 37°C. Cells were washed in 1× wash buffer B, followed by 0.01× wash buffer B. Hoechst 33258 (1 µg/ml, H3569, Thermo Fisher Scientific) was used to stain cellular nuclei. Images were obtained on a Zeiss LSM 880 laser scanning confocal microscope. To quantify the percentage of cells with PLA signal, the number of GFP-(GR)₁₀₀-positive cells containing PLA signal was counted in a blinded fashion from 14-18 images.

Immuno- electron microscopy

To examine the ultrastructure of poly(GR) aggregates, immuno- electron microscopy (IEM) was performed as previously described (21). Rabbit polyclonal anti-poly(GR) antibody (7810, 1:20) (10) was used as a primary antibody and goat anti-rabbit IgG conjugated with 18 nm colloidal gold particles (1:20, Jackson ImmunoResearch Laboratories) was used as the secondary antibody. Thin sections stained with uranyl acetate and lead citrate were examined with a Philips 208S electron microscope (FEI) fitted with a Gatan 831 Orius CCD camera (Gatan).

Human tissues

Post-mortem hippocampal and frontal cortical tissues from frontotemporal dementia (FTD) and amyotrophic lateral sclerosis (ALS) patients with the *C9orf72* repeat expansion were obtained from the Mayo Clinic Florida Brain Bank. Information on human patients is provided in **Table S3**. Written informed consent was obtained before study entry from all subjects or their legal next of kin if they were unable to give written consent, and biological samples were obtained with Mayo Clinic Institutional Review Board (IRB) approval.

Animal studies

All procedures using mice were performed in accordance with the National Institutes of

Health Guide for Care and Use of Experimental Animals and approved by the Mayo Clinic Institutional Animal Care and Use Committee (IACUC).

Virus production

rAAV9 virus was produced as previously described (13, 14, 29). Briefly, AAV vectors expressing GFP, GFP-(GR)₂₀₀, (G₄C₂)₂ or (G₄C₂)₁₄₉ were co-transfected with helper plasmids in HEK293T cells using polyethylenimine (23966, Polysciences, Inc.). Cells were harvested forty-eight hours following transfection, and lysed in the presence of 0.5% sodium deoxycholate and 50 Units/mL Benzonase (Sigma-Aldrich) by freeze-thawing. The virus was isolated using a discontinuous iodixanol gradient. The genomic titer of each virus was determined by qRT-PCR, and AAV solutions were diluted in sterile phosphate-buffered saline (PBS).

Neonatal viral injections

Intracerebroventricular (ICV) injections of virus were performed as previously described (13, 14, 29). Briefly, 2 μ l (1×10^{10} genomes/ μ l) of AAV-GFP, AAV-GFP-(GR)₂₀₀, AAV-(G₄C₂)₂ or AAV-(G₄C₂)₁₄₉ solution was manually injected into each lateral ventricle of cryoanesthetized C57BL/6J mouse pups on postnatal day 0 (P0). Pups were allowed to recover from cryoanesthesia on a heating pad, and were then returned to the home cage with the mother.

Antisense oligonucleotide (ASO) injections and sample collection

PBS or c9ASO was injected into the central nervous system of 3 month-old AAV-(G₄C₂)₂ or AAV-(G₄C₂)₁₄₉ mice by means of stereotactic ICV injection, as previously described (34) with some minor modifications. The c9ASO targeting the G₄C₂ repeat expansion (CGGCCCGGCCCGGC), developed and provided by Ionis Pharmaceuticals, was a MOE-gaper ASO with 16 nucleotides in length, wherein the central gap segment comprising eight 2'-deoxyribonucleotides (DNA) that are flanked on the 5' and 3' wings by four 2'-O-methoxyethyl (MOE) modified nucleotides. Internucleotide linkages are phosphorothioate interspersed with phosphodiester, and all cytosine residues are 5'-methylcytosines. Specifically, 10 μ l of PBS or c9ASO solution (corresponding to 350 μ g ASOs) were delivered into the right lateral ventricle using the coordinates: 0 mm anterior and 1.0 mm lateral to the right from bregma, and 1.9-2.0 mm deep as measured from the brain surface. PBS-treated AAV-(G₄C₂)₂ mice (n = 17) or AAV-(G₄C₂)₁₄₉ mice (n = 18), and c9ASO-treated AAV-(G₄C₂)₁₄₉ (n = 12) mice were compared.

Tissue processing

For protein, immunostaining and RNA analyses, the mice were euthanized by CO₂ or ketamine/xylazine through intraperitoneal injection. Blood samples were then collected by cardiac puncture, and mice euthanized by exsanguination followed by transcardial perfusion with saline. Then, brains were harvested and cut sagittally across the midline. The brain was rapidly removed and hemisected. Sagittal half brains were immersion fixed in 4% paraformaldehyde, embedded in paraffin, sectioned (5 μ m thick), and then mounted on glass slides for immunofluorescence or immunohistochemistry staining. The other half brains were dissected

and frozen (cortex, hippocampus, subcortex, midbrain, brainstem, and cerebellum frozen separately).

Immunohistochemistry staining

Sagittal half brains fixed in 4% paraformaldehyde were embedded in paraffin, sectioned at 5 μm , and mounted on positively-charged glass slides. After drying overnight, paraffin sections were deparaffinized in xylene, and rehydrated through a series of ethanol solutions, followed by washing in dH₂O. Antigen retrieval was performed by steaming slides in dH₂O or Tris-EDTA (DAKO), pH 9.0 for 30 minutes followed by a 5 minute incubation in Dako Peroxidase Block (S2001, DAKO) to block endogenous peroxidase activity. To detect the sense DPR proteins, sections were immunostained with primary antibody (**Table S2**) using the DAKO Autostainer (Universal Staining System) and the DAKO+HRP system. To detect ataxin-2 or NeuN, slides were blocked with Dako Protein Block Serum-Free (X0909, DAKO) for 1 hour, and incubated with primary antibody (**Table S2**) for 45 minutes. After washing, sections were incubated for 30 minutes in Dako Envision-Plus anti-rabbit (K4003, DAKO) or anti-mouse (K4001, DAKO) labeled HRP polymer, respectively. Peroxidase labeling was visualized with the Liquid DAB + Substrate Chromogen System (K3468, DAKO).

To detect pTDP-43 in AAV-(G₄C₂)₁₄₉ mice or poly(GR) in AAV-GFP-(GR)₂₀₀ mice, slides were deparaffinized and rehydrated as described above, and antigen retrieval was performed by steaming in sodium citrate buffer (10 mM sodium citrate, 0.05% Tween-20, pH 6.0) for 30 minutes. After cooling and washing with dH₂O, slides were incubated with Dako Dual Endogenous Enzyme Block (DAKO), and subsequently washed in PBS. Sections were then blocked with 2% normal goat serum for 1 hour, followed by an overnight incubation with primary antibody (**Table S2**) at 4°C. The next day, slides were washed with PBS, incubated with biotinylated goat anti-rabbit or rabbit anti-rat secondary (1:200) for 2 hours, and again washed in PBS. Slides were then incubated with avidin-biotin complex solution for 30 minutes, washed in PBS, and reacted with 3,3'-diaminobenzidine (Acros Organics) activated with hydrogen peroxide, with the reaction stopped by rinsing slides in dH₂O.

Following labeling, all sections were counterstained with hematoxylin (Thermo Fisher Scientific), dehydrated through ethanol and xylene washes, and cover-slipped with Cytoseal mounting medium (Thermo Fisher Scientific). Slides were scanned with a ScanScope AT2 (Leica Biosystems), and representative images taken with ImageScope software (v12.1; Leica Biosystems).

Immunofluorescence staining in mouse and human brains

Paraffin sections (5 μm) of mouse and human brain tissues were deparaffinized, rehydrated, steamed for 30 minutes in Dako antigen retrieval solution, blocked with Dako All Purpose Blocker for 1 hour, and incubated with primary antibody (**Table S2**). After washing, sections were incubated with corresponding Alexa Fluor 488-, 568- or 647-conjugated donkey

anti-species (1:500, Molecular Probes) for 2 hours. Hoechst 33258 (1 µg/ml, Thermo Fisher Scientific) was used to stain cellular nuclei. Images were obtained on a Zeiss LSM 880 laser scanning confocal microscope.

Quantification of neuropathology

To quantify diffuse and aggregated poly(GR), high resolution digitized images of immunostained slides were obtained by using a ScanScope AT2 (Leica Biosystems). The cortex was annotated on mid-sagittal serial sections. The number of diffuse and aggregated poly(GR) was quantified manually in a blinded fashion. To quantify pTDP-43 inclusions, high resolution digitized images of immunostained slides were obtained by using a ScanScope AT2 (Leica Biosystems). The cortex was annotated on mid-sagittal serial sections. The number of pTDP-43 inclusions was quantified manually in a blinded fashion. To quantify TDP-43, KPNA2 and NUP98 pathology, non-transduced (NT), diffuse poly(GR) or aggregated poly(GR) cells exhibiting TDP-43, KPNA2 and NUP98 pathology were counted in a unblinded fashion in the cortex of 2-week-old mice expressing GFP-(GR)₂₀₀ (TDP-43: ~180–250 cells were counted per mouse; KPNA2: ~150–240 cells were counted per mouse; NUP98: ~140–170 cells were counted per mouse). To quantify abnormal co-localization of NPC with either TDP-43 or eIF3η, non-transduced (NT), diffuse poly(GR) or aggregated poly(GR) cells exhibiting abnormal co-localization of NPC with either TDP-43 or eIF3η were counted in a unblinded fashion in the cortex of 2-week-old mice expressing GFP-(GR)₂₀₀ (NPC and eIF3η: ~170–220 cells were counted per mouse; NPC and TDP-43: ~180–220 cells were counted per mouse). To quantify co-localization of poly(GA) with TDP-43 and eIF3η in the cortex of 3-month-old mice expressing GFP-(GA)₅₀, ~90–120 poly(GA) inclusions were counted per mouse. To quantify co-localization of TDP-43 with poly(GA) or poly(GR), the total number of poly(GA) or poly(GR) inclusions, as well as the number of inclusions that were also positive for TDP-43 were counted in a blinded fashion in the hippocampus of c9FTD/ALS patients [poly(GA): ~90–470 inclusions were counted per patient; poly(GR): ~35–180 inclusions were counted per patient].

RNA Fluorescence In Situ Hybridization (FISH)

The RNA FISH protocol was performed as previously described (13). Briefly, tissue sections were deparaffinized and rehydrated through a series of xylene and ethanol solutions, permeabilized with ice cold 2% acetone/1× DEPC-PBS, washed with DEPC-H₂O, and then dehydrated in ethanol. To detect sense RNA foci, sections were incubated with pre-hybridization buffer [50% formamide (Midsci), 10% dextran sulfate (Millipore), 2× saline-sodium citrate buffer (SSC), 50 mM sodium phosphate buffer pH 7.0] for 20–30 minutes at 66°C, and then hybridized for 24 hours at 66°C in a dark, humidified chamber with a fluorescently-labeled locked nucleic acid (LNA) probe (5) [TYE563-(CCCCGGCCCCGGCCCC); Exiqon product number 500150, design id: 283117] diluted to a final concentration of 40 nM. Next, sections were washed with 2× SSC/0.1% Tween-20 at room temperature for 5 minutes, and then washed

twice with pre-warmed 0.2× SSC at 60°C for 10 minutes in the dark. Following these washes, slides were coverslipped using Vectashield mounting media with DAPI (Vector Laboratories). Representative images of sense RNA foci in the cortex were taken with an AxioImager Z1 fluorescent microscope (Carl Zeiss MicroImaging). RNA foci burden was quantified in a blinded fashion by calculating the percentage of cells in the motor cortex (from 300–400 cells total) containing sense RNA foci.

RNA extraction, reverse transcription and qPCR

For RNA extraction, frozen hippocampi were homogenized in Trizol LS (250 µL), and total RNA extracted using the Direct-zol RNA MiniPrep kit (Zymo Research) according to manufacturer's instructions. cDNA was then obtained following reverse transcription of 250 ng of the extracted RNA with random primers and the High Capacity cDNA Transcription Kit (Applied Biosciences). qRT-PCR was performed in triplicate for all samples using the SYBR green assay (Life Technologies) on an ABI Prism 7900HT Fast Real-Time PCR System (Applied Biosystems). As the AAV-(G₄C₂)₁₄₉ vector contains 119 base pairs of human flanking sequence 5' of the G₄C₂ repeat, primers were designed targeting this region to assess mRNA expression of exogenous, AAV-derived G₄C₂-containing transcripts. Endogenous *Gapdh* and *Rplp0* mRNA were also quantified. The sequences of the primers used for this study are listed in **Table S4**. Relative mRNA expression of the G₄C₂ 5' flanking sequence was normalized to the geometric mean of the endogenous transcript controls, *Gapdh* and *Rplp0*.

Immunoassay analysis of poly(GR), poly(GA), and poly(GP)

Frozen cortex samples were homogenized in co-immunoprecipitation buffer (50 mM Tris-HCl, pH 7.4, 300 mM NaCl, 1% Triton X-100, 5 mM EDTA) containing protease and phosphatase inhibitors. After sonication, the lysates were centrifuged at 16,000 × g for 20 minutes, and BCA assay performed on the supernatant to determine protein concentration. Previously characterized Meso Scale Discovery (MSD) sandwich immunoassays were then used to detect poly (GR) (29), or poly(GP) and poly(GA) (49). In brief, lysates were diluted in Tris-buffered saline (TBS) and an equal amount of protein for all samples was tested in duplicate wells. Response values corresponding to the intensity of emitted light upon electrochemical stimulation of the assay plate using the MSD QUICKPLEX SQ120 were acquired and background corrected using the average response from lysates obtained from control (G₄C₂)₂ mice.

Detection of neurofilament light (NfL) in plasma

Blood samples from mice were collected in EDTA tubes, and centrifuged to obtain plasma. Plasma NfL concentrations were then determined using a Simoa NF-Light Advantage Kit (102258) run on the automated HD-1 Analyzer (Quanterix) per the manufacturer's protocol. Briefly, plasma samples were diluted 1:4 at the bench, and subsequently transferred to 96-well plates along with calibrators, two quality control samples, and five interassay controls with a

range of known NfL concentrations. NfL concentrations were then interpolated from the standard curve using a 4 parameter logistic curve fit ($1/y^2$ weighted).

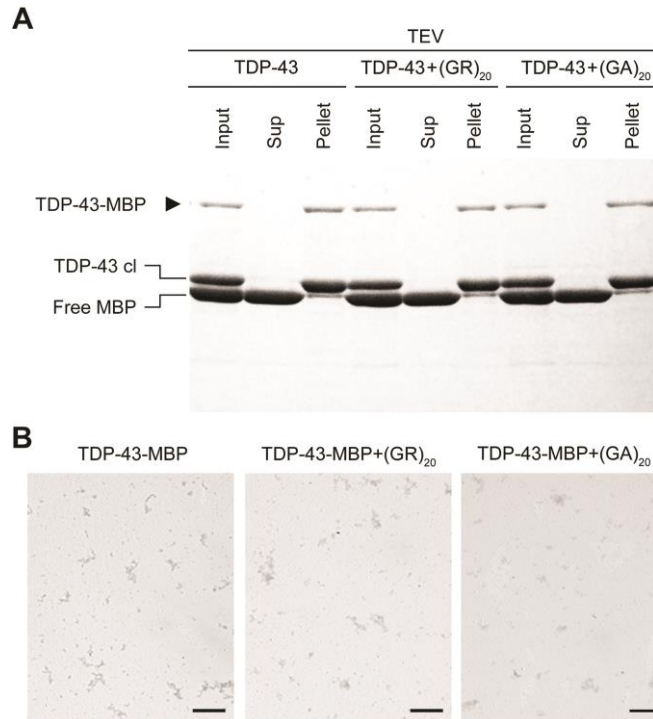


Fig. S1. Poly(GR) accelerates and enhances TDP-43 aggregation. (A) Sedimentation of TDP-43 (5 μ M) in the absence or presence of 2 μ M poly(GR) or poly(GA). Samples were sedimented at the end-point of the aggregation assay ($t = 16$ hours). (B) Representative electron micrographs of TDP-43 (5 μ M) in the absence or presence of 2 μ M poly(GR) or poly(GA), without TEV protease. Scale bar, 2 μ m.

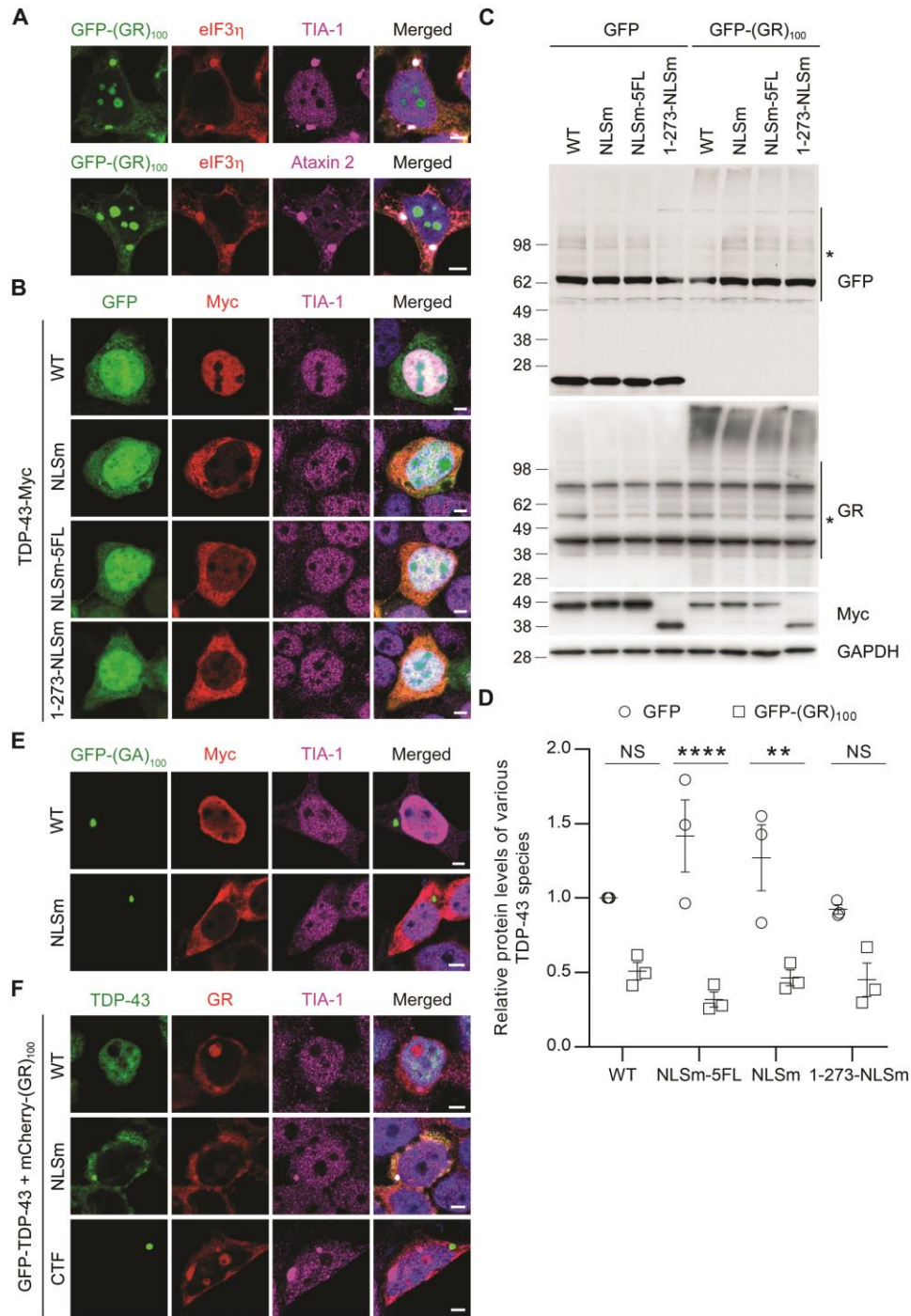


Fig. S2. Poly(GR) mediates sequestration of cytosolic full-length TDP-43 into the inclusions.

(A) Triple-immunofluorescence staining for GFP-(GR)₁₀₀, eIF3η and TIA-1 or Ataxin 2 in HEK293T cells expressing GFP-(GR)₁₀₀. Scale bars, 5 μm. (B) Triple-immunofluorescence staining for GFP, TDP-43-Myc and TIA-1 in HEK293T cells expressing GFP and Myc-tagged TDP-43 species. Scale bars, 5 μm. (C) Western blot confirming expression of GFP, GFP-(GR)₁₀₀ and TDP-43-Myc in HEK293T cells co-transfected with either GFP or GFP-(GR)₁₀₀ and various

Myc-tagged TDP-43 species. GAPDH was used to control for protein loading. * Indicates non-specific bands. **(D)** Densitometric analysis of Myc-tagged TDP-43 species in HEK293T cells co-expressing various Myc-tagged TDP-43 constructs with either GFP or GFP-(GR)₁₀₀ (n = 3 independent experiments). **(E)** Triple-immunofluorescence staining for poly(GA), TDP-43 and TIA-1 in HEK293T cells expressing GFP-(GA)₁₀₀ and Myc-tagged TDP-43 constructs [including wild-type (WT) and nuclear localization signal mutant (NLSm)] (n = 3 independent experiments). Scale bars, 5 μ m. **(F)** Triple-immunofluorescence staining for GFP-TDP-43, mCherry-(GR)₁₀₀, and TIA-1 in HEK293T cells co-transfected with mCherry-(GR)₁₀₀ and GFP-tagged TDP-43 species [including WT, NLSm, and the C-terminal fragment (CTF)]. Scale bars, 5 μ m. Data shown as the mean \pm SEM. ** $P = 0.0016$, **** $P < 0.0001$, NS (left to right) $P = 0.0590$, and $P = 0.0726$, two-way ANOVA, Tukey's post hoc analysis.

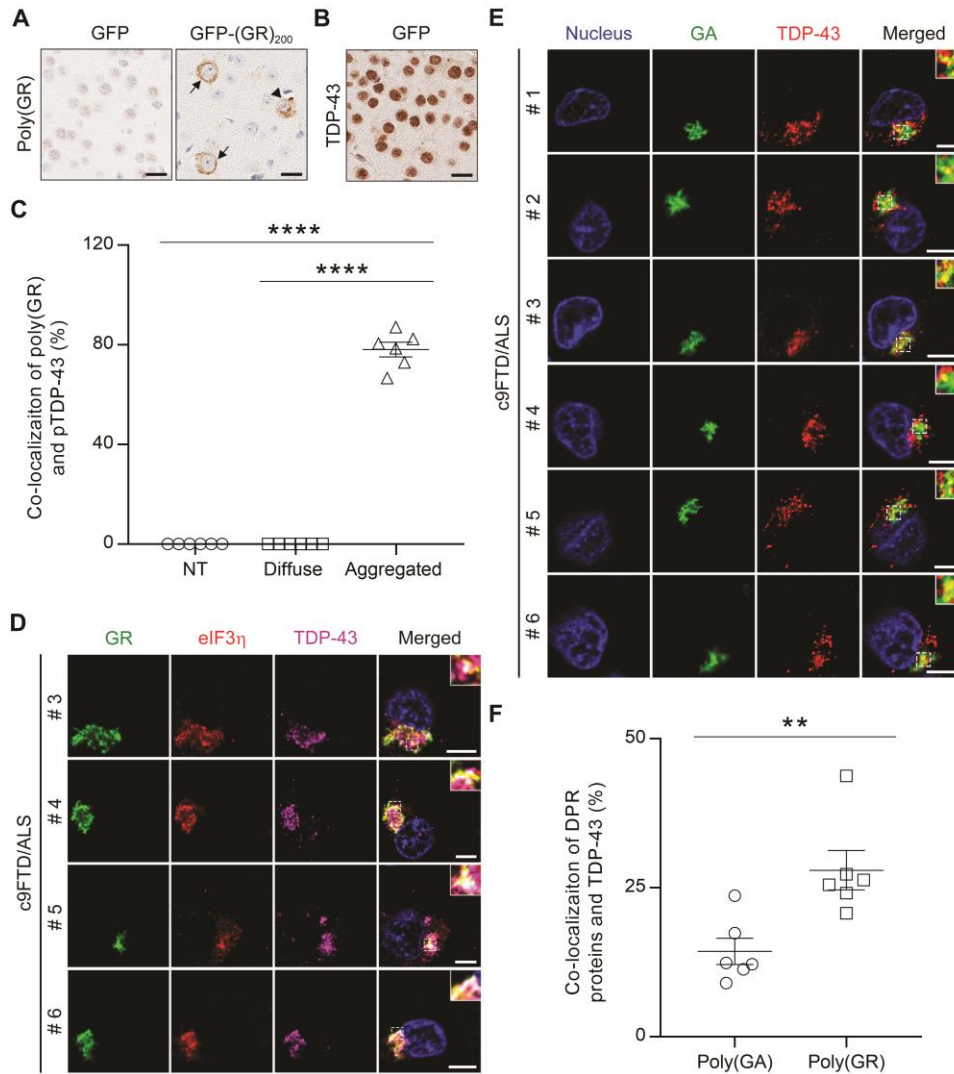


Fig. S3. TDP-43 and DPR burden in mouse and human. (A) Representative images of immunohistochemical analysis of poly(GR) in the cortex 3-month-old GFP or GFP-(GR)₂₀₀ mice (diffuse labeling noted by black arrows, aggregates indicated by black arrowheads). Scale bar, 20 μ m. (B) Representative images of immunohistochemical analysis of TDP-43 in the cortex of 2-week-old GFP mice. Scale bar, 20 μ m. (C) Quantification of the percentage of co-localization between poly(GR) and pTDP-43 in either non-transduced (NT) or transduced cells with diffuse or aggregated poly(GR) (n =6). (D) Triple-immunofluorescence staining for poly(GR), eIF3 η , and TDP-43 in the hippocampus of c9FTD/ALS patients (see Table S3 for patient information). Scale bars, 5 μ m. (E) Double-immunofluorescence staining for poly(GA) and TDP-43 in the hippocampus of c9FTD/ALS patients (see Table S3 for patient information). Scale bars, 5 μ m. (F) Quantification of the percentage of co-localization between TDP-43 and either poly(GA) or poly(GR) in c9FTD/ALS patient tissue. Data shown as the mean \pm SEM. In (B), **** $P < 0.0001$, one-way ANOVA, Tukey's post hoc analysis. In (F), ** $P = 0.0064$, two-tailed unpaired t test.

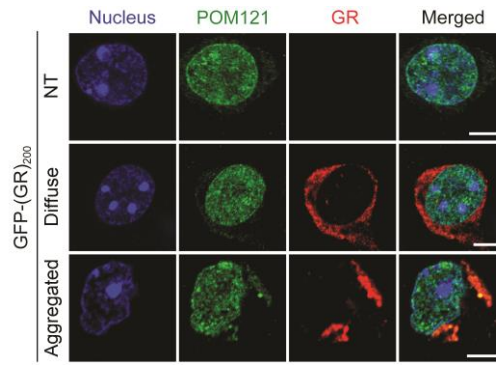


Fig. S4. Poly(GR) aggregates sequester nuclear pore POM121 protein in vivo. Double-immunofluorescence staining for poly(GR) and POM121 in the cortex of 2-week-old GFP-(GR)₂₀₀ mice (n = 6). Scale bars, 5 μ m.

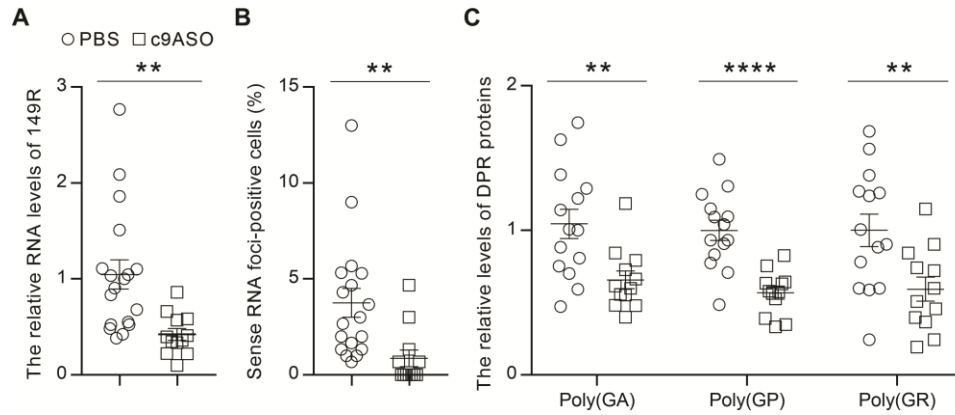


Fig. S5. c9ASO reduces G₄C₂ repeat-containing RNA and sense DPR protein burden. (A) qRT-PCR analysis of exogenous G₄C₂ repeat RNA transcripts in (G₄C₂)₁₄₉ mice using human-specific primers 5' of the repeat targeting sequence present in the AAV vector. Exogenous G₄C₂ repeat mRNA expression was normalized to the geometric mean of the endogenous controls *Gapdh* and *Rplp0* (PBS, n = 18; c9ASO, n = 12). (B) Percentage of cells containing sense RNA foci in the motor cortex of PBS (n = 19) or c9ASO-treated (n = 12) (G₄C₂)₁₄₉ mice. (C) Poly(GA), poly(GP) and poly(GR) concentrations in brain lysates from PBS (n = 14) or c9ASO-treated (n = 12) (G₄C₂)₁₄₉ mice were measured by immunoassay. Data presented as the mean ± SEM. In (A), ** *P* = 0.0033, unpaired two-tailed *t*-test. In (B), ***P* = 0.0066, unpaired two-tailed *t*-test. In (C), ** (left to right) *P* = 0.0045, *P* = 0.0089 and *****P* < 0.0001, unpaired two-tailed *t*-test.

Table S1. cDNA sequence of the GFP-(GR)₂₀₀ and mCherry-(GR)₁₀₀ plasmids.

GFP-(GR)₂₀₀ plasmid

ATGGTGAGCAAGGGCGAGGAGCTGTTACCGGGGTGGTGCCCATCCTGGTCGAGC
TGGACGGCGACGTAAACGGCCACAAGTTCAGCGTGTCCGGCGAGGGCGAGGGCG
ATGCCACCTACGGCAAGCTGACCCTGAAGTTCATCTGCACCACCGGCAAGCTGCC
CGTGCCCTGGCCCACCCTCGTGACCACCCTGACCTACGGCGTGCAGTGCTTCAGCC
GCTACCCCGACCACATGAAGCAGCACGACTTCTTCAAGTCCGCCATGCCCGAAGG
CTACGTCCAGGAGCGCACCATCTTCTTCAAGGACGACGGCAACTACAAGACCCGC
GCCGAGGTGAAGTTCGAGGGCGACACCCTGGTGAACCGCATCGAGCTGAAGGGCA
TCGACTTCAAGGAGGACGGCAACATCCTGGGGCACAAGCTGGAGTACA ACTACAA
CAGCCACAACGTCTATATCATGGCCGACAAGCAGAAGAACGGCATCAAGGTGAAC
TTCAAGATCCGCCACAACATCGAGGACGGCAGCGTGCAGCTCGCCGACC ACTACC
AGCAGAACACCCCATCGGCGACGGCCCCGTGCTGCTGCCCGACAACCACTACCT
GAGCACCCAGTCCGCCCTGAGCAAAGACCCCAACGAGAAGCGCGATCACATGGTC
CTGCTGGAGTTCGTGACCGCCGCCGGGATCACTCTCGGCATGGACGAGCTGTACA
AGTCCGGACTCAGATCTCGAGCTCAAGCTTCG**GGCCGCGGCCGTGGTCGCGGTTCG**
TGGACGTGGCCGTGGCCGTGGCCGAGGTTCGCGGTTCGGGGACGTGGCCGTGGTCGT
GGCCGAGGTCGAGGTCGCGGACGTGGACGTGGTCGAGGTCGGGGACGTGGACGA
GGCCGTGGTCGTGGCCGAGGTCGCGGACGTGGGCGAGGTCGCGGTTCGAGGCCGGG
GACGTGGCCGTGGTCGTGGACGGGGACGGGGTCGGGGACGCGGTTCGAGGCCGTG
GACGTGGACGGGGTCGAGGACGTGGACGTGGTCGTGGACGTGGCCGTGGACGTGG
ACGCGGCCCGCGGCCGTGGTCGCGGTTCGTGGACGTGGCCGTGGCCGTGGCCGAGGT
CGCGGTTCGGGGACGTGGCCGTGGTCGTGGCCGAGGTCGAGGTCGCGGACGTGGAC
GTGGTCGAGGTCGGGGACGTGGACGAGGCCGTGGTCGTGGCCGAGGTCGCGGACG
TGGGCGAGGTCGCGGTTCGAGGCCGGGGACGTGGCCGTGGTCGTGGACGGGGACG
GGGTCGGGGACGCGGTTCGAGGCCGTGGACGTGGACGGGGTCGAGGACGTGGACG
TGGTCGTGGACGTGGCCGTGGACGTGGACGCGGCCCGCGGCCGTGGTCGCGGTTCG
GGACGTGGCCGTGGCCGTGGCCGAGGTCGCGGTTCGGGGACGTGGCCGTGGTCGTG
GCCGAGGTCGAGGTCGCGGACGTGGACGTGGTCGAGGTCGGGGACGTGGACGAG
GCCGTGGTCGTGGCCGAGGTCGCGGACGTGGGCGAGGTCGCGGTTCGAGGCCGGGG
ACGTGGCCGTGGTCGTGGACGGGGACGGGGTCGGGGACGCGGTTCGAGGCCGTGG
ACGTGGACGGGGTCGAGGACGTGGACGTGGTCGTGGACGTGGCCGTGGACGTGGA
CGCGGCCGTGGTCGCGGTTCGTGGACGTGGCCGTGGCCGTGGCCGAGGTCGCGGTTC
GGGGACGTGGCCGTGGTCGTGGCCGAGGTCGAGGTCGCGGACGTGGACGTGGTCG
AGGTCGGGGACGTGGACGAGGCCGTGGTCGTGGCCGAGGTCGCGGACGTGGGCG
AGGTCGCGGTTCGAGGCCGGGGACGTGGCCGTGGTCGTGGACGGGGACGGGGTCG
GGGACGCGGTTCGAGGCCGTGGACGTGGACGGGGTCGAGGACGTGGACGTGGTCG
TGGACGTGGCCGTGGACGTGGACGGTAG

The (GR)₂₀₀ sequence is highlighted in yellow

mCherry-(GR)₁₀₀ plasmid

ATGGTGAGCAAGGGCGAGGAGGATAACATGGCCATCATCAAGGAGTTCATGCGCT
TCAAGGTGCACATGGAGGGCTCCGTGAACGGCCACGAGTTCGAGATCGAGGGCGA
GGGCGAGGGCCGCCCTACGAGGGCACCCAGACCGCCAAGCTGAAGGTGACCAA
GGGTGGCCCCCTGCCCTTCGCCTGGGACATCCTGTCCCCTCAGTTCATGTACGGCT

CCAAGGCCTACGTGAAGCACCCCGCCGACATCCCCGACTACTTGAAGCTGTCCTTC
CCCGAGGGCTTCAAGTGGGAGCGCGTGATGAACTTCGAGGACGGCGGCGTGTTGA
CCGTGACCCAGGACTCCTCCCTGCAGGACGGCGAGTTCATCTACAAGGTGAAGCT
GCGCGGCACCAACTTCCCCTCCGACGGCCCCGTAATGCAGAAGAAGACCATGGGC
TGGGAGGCTCCTCCGAGCGGATGTACCCCGAGGACGGCGCCCTGAAGGGCGAGA
TCAAGCAGAGGCTGAAGCTGAAGGACGGCGGCCACTACGACGCTGAGGTCAAGA
CCACCTACAAGGCCAAGAAGCCCGTGCAGCTGCCCGGCGCCTACAACGTCAACAT
CAAGTTGGACATCACCTCCCACAACGAGGACTACACCATCGTGGAACAGTACGAA
CGCGCCGAGGGCCGCCACTCCACCGGCGGCATGGACGAGCTGTACAAGGAAGCTT
CGGGCCGCGGCCGTGGTCGCGGTCGTGGACGTGGCCGTGGCCGTGGCCGAGGTTCG
CGGTTCGGGGACGTGGCCGTGGTCGTGGCCGAGGTTCGAGGTTCGCGGACGTGGACGT
GGTCGAGGTTCGGGGACGTGGACGAGGCCGTGGTCGTGGCCGAGGTTCGCGGACGTG
GGCGAGGTTCGCGGTCGAGGCCGGGGACGTGGCCGTGGTCGTGGACGGGGACGGG
GTCGGGGACGCGGTCGAGGCCGTGGACGTGGACGGGGTTCGAGGACGTGGACGTG
GTCGTGGACGTGGCCGTGGACGTGGACGCGGCCGTGGTCGCGGTCGTGGACGTGG
CCGTGGCCGTGGCCGAGGTTCGCGGTCGGGGACGTGGCCGTGGTCGTGGCCGAGGT
CGAGGTTCGCGGACGTGGACGTGGTCGAGGTTCGGGGACGTGGACGAGGCCGTGGTC
GTGGCCGAGGTTCGCGGACGTGGGCGAGGTTCGCGGTCGAGGCCGGGGACGTGGCC
GTGGTCGTGGACGGGGACGGGGTCGGGGACGCGGTCGAGGCCGTGGACGTGGAC
GGGGTCGAGGACGTGGACGTGGTCGTGGACGTGGCCGTGGACGTGGACGGTAG

The (GR)₁₀₀ sequence is highlighted in yellow.

Table S2. Primary antibodies for Western blot, immunohistochemistry, and immunofluorescence staining.

Western blot				
Antibody	Species	Dilution	Number	Company
anti-GR	rabbit	1:2000	Rb7810 ^a	
anti-GFP	rabbit	1:4000	A-6455	Life Technologies
anti-Myc	mouse	1:1000	MA1-980	Invitrogen
anti-GAPDH	mouse	1:5000	H86504M	Meridian Life Science
Immunohistochemistry				
Antibody	Species	Dilution	Number	Company
anti-GA	rabbit	1:50000	Rb9880 ^a	
anti-GP	rabbit	1:10000	Rb5823 ^a	
anti-GR	rabbit	1:2500	Rb7810 ^a	
anti-pTDP-43	rabbit	1:1000	Rb3655 ^b	
anti-TDP-43	rabbit	1:1000	MC2079 ^c	
anti-GR	rat	1:250	MABN778	EMD Millipore
anti-Ataxin 2	rabbit	1:500	21776-1-AP	Proteintech
Immunofluorescence				
Antibody	Species	Dilution	Number	Company
anti-Myc	mouse	1:1000	MA1-980	Invitrogen
anti-TIA-1	rabbit	1:2000	ab40693	Abcam
anti-eIF3 η	goat	1:200	sc-16377	Santa Cruz Biotechnology
anti-GR	rabbit	1:2000	Rb7810 ^a	Cosmo Bio
anti-GR	rabbit	1:500	MABN778	EMD Millipore
Anti-pTDP-43	rabbit	1:1000	CAC-TIP-PTD-P02	Cosmo Bio
anti-Ataxin 2	rabbit	1:500	21776-1-AP	Proteintech
anti-NPC	mouse	1:100	ab24609	Abcam
anti-NUP98	rat	1:200	ab50610	Abcam
anti-POM121	rabbit	1:100	PA5-36498	Invitrogen
anti-RanGAP1	rabbit	1:100	sc-25630	Santa Cruz Biotechnology
anti-GA	mouse	1:500	MABN889	EMD Millipore
anti-GFP	mouse	1:1000	33-2600	Invitrogen
anti-TDP-43	rabbit	1:1000	MC2079 ^c	
Importin α 5	rabbit	1:100	18137-1-AP	Proteintech
KPNA2	rabbit	1:100	0819-1-AP	Proteintech

^{a, d}Antibody described in: T. F. Gendron *et al.*, *Acta Neuropathol* **126**, 829-844 (2013).

^bAntibody described in: J. Chew *et al.*, *Science* **348**, 1151-1154 (2015).

^cAntibody described in: Y. J. Zhang *et al.*, *Proc Natl Acad Sci U S A.* **106**, 7607-7612 (2009).

Table S3. Characteristics of patients with c9FTD/ALS.

Case #	Pathological Diagnosis	Gender	Age at Onset	Age at death	Disease Duration	<i>C9orf72</i> repeat expansion
1	FTLD/ALS	F	60.4	61.4	1.0	Yes
2	FTLD	M	62	73.0	11.0	Yes
3	FTLD/ALS	F	52	60.3	8.3	Yes
4	FTLD/ALS	M	57	62.2	5.2	Yes
5	FTLD	M	68	73.9	5.9	Yes
6	FTLD/ALS	M	57	62	6.0	Yes

FTLD, frontotemporal lobar degeneration; ALS, amyotrophic lateral sclerosis

Table S4. Primers for qPCR.

Model	Target	Primers
mouse brain	5' flanking sequence	5'-TAGTACTCGCTGAGGGTGAAC-3' 5'-CTACAGGCTGCGGTTGTTTC-3'
mouse brain	<i>Gfap</i>	5'-CATGGCCTTCCGTGTTCCCTA-3' 5'-CCTGCTTCACCACCTTCTTGAT-3'
mouse brain	<i>Rplp0</i>	5'-ACTGGTCTAGGACCCGAGAAG-3' 5'-CTCCCACCTTGTCTCCAGTC-3'

Data file S1. Raw data for all the quantitative figures where $n < 20$.
Provided as a separate Excel file.